# Chromatin Mechanics: Starting Local, Going Global

Submitted in partial fulfillment of the requirements for

the degree of

Doctor of Philosophy

in

Department of Biomedical Engineering

Daniel B. Whitefield

B.S., Biology, Lubbock Christian University
B.S., Chemistry, Lubbock Christian University
B.S., Mathematics, Lubbock Christian University

Carnegie Mellon University
Pittsburgh, PA

July 2021

# Acknowledgements

I would like to thank all past and present members of the Dahl Laboratory for their instruction, feedback, help, and support during the course of my Master's and Ph.D. work.

This research was supported by the Biomechanics in Regenerative Medicine (BiRM) program - BiRM NIH Training Grant – 5 T32 EB 3392-14 (Daniel B. Whitefield), Progeria Research Foundation (Kris N. Dahl), NSF CMMI-1634888, CMMI-1634888, NIH-F30AG, NIBIB-T32, NIGMS-T32, NSERC, NDSEG. NSF-CMMI 1300476 (Kris N. Dahl), NIH-GM118833 to (Li Lan), and NIH-EB003392 to (Travis J. Armiger).

## Doctoral Committee:

I would like to thank my Ph.D. Thesis Committee members especially for their guidance, insight, and encouragement during the course of my work at Carnegie Mellon University. Their advice, both scientific and professional, proved crucial to my success as a doctoral student and in my development as a professional researcher.

Kris Noel Dahl, Ph.D.

Committee Chair

Professor of Chemical Engineering, Biomedical Engineering, and Materials Science and Engineering, Carnegie Mellon University

Phil G. Campbell, Ph.D.

Research Professor of Biomedical Engineering, Engineering Research Accelerator, Biological Sciences, and Materials Science & Engineering, Carnegie Mellon University

Xi (Charlie) Ren, Ph.D.

Assistant Professor of Biomedical Engineering, Carnegie Mellon University

Fred L. Homa, Ph.D.

Professor of Microbiology and Molecular Genetics, University of Pittsburgh

Patricia Lynn Opresko, Ph.D.

Professor of Environmental and Occupational Health, University of Pittsburgh

# Abstract

Exogenous Chromatin Damage or Alteration, or CDA, represents an existential threat to the viability of the cell. It is important to understand the cause of various types of CDA, the direct effect that they have upon the chromatin, and the cell's natural response in order to either counteract them, in the case of disease or injury, or amplify them in a targeted manner, in the case of cancer treatment. One of the main challenges to overcome is the complexity of biology. One way to simplify this complexity is the use of an orthogonal method, such as measuring the mechanical properties of the system, that takes into account all the individual contributions simultaneously without parsing them out individually. Analogous to this is the way an integral finds the area under a strangely shaped curve by summing an infinite number of infinitesimally thin slices. Directly measuring the motion of chromatin will allow us to study the effect of a particular CDA upon the chromatin without individually measuring the contributions of many participating proteins or pathways. We have specialized in one particular method to accomplish this goal called Sensors from IntraNuclear Kinetics (SINK). Here we demonstrate how SINK can be used to study CDA in vastly different contexts. We begin with site-specific DNA damage (Chapter III) and expand to widespread DNA damage due to chemotherapeutic treatment (Chapter IV). Next, we examine total nuclear remodeling due to viral infection (Chapter V), then move on to remodeling of both chromatin and cytoskeleton for genome-wide damage prevention in response to mechanical stimulus (Chapter VI). We find that SINK allows us to detect patterns other methods could not, which improves our understanding of processes that are already well-studied and enables us to make new discoveries about phenomena that have previously been difficult to study.

# Table of Contents

# List of Figures and Illustrations

# Chapter I

## Introduction

Chromatin is a highly organized network made up of DNA and proteins located inside the nuclei of eukaryotic cells.[1,2,3] The primary purpose of chromatin is to store biologically encoded information for the production of proteins in the form of genes and to make that information available at the proper time and in the proper amounts.[1,2,3] The organization and structure of the chromatin network is pivotal in achieving this goal. Properly organized chromatin is capable of integrating both chemical and mechanical stimuli and responding with appropriate gene expression.[1,3] Improperly organized chromatin can lead to a pathological response to stimuli.[3] It is important to understand proper chromatin organization and how that organization may be disrupted in order to develop strategies to either remedy faulty organization in a disease state or induce faulty organization in a targeted manner when treating cancer. A vast amount of research has been devoted to understanding chromatin response to chemical stimuli, and recently an increasing amount of research is being done to better understand the chromatin response to mechanical stimuli. An arsenal of tools exists to investigate the effects of chemical stimuli and many of those tools can be quite specific in targeting particular proteins or DNA sequences participating in an interaction. However, methods of interrogating mechanical interactions are more limited in number and specificity. Here, we describe a method of probing mechanical processes that is robust enough to allow study of changes to mechanics at multiple levels of specificity – from highly targeted at a particular gene locus to a particular regime of chromatin organization to the entire chromatin network. Sensors from IntraNuclear Kinetics (SINK) is a fluorescence microscopy particle tracking technique that uses chromatin-bound fluorescently-

tagged probes to measure chromatin motion and, in some circumstances, can measure the relative prevalence of certain molecular processes such as chromatin condensation and force propagation via molecular motor activity.[4,5,6,7,8,9]

## Chromatin Structure and Organization

Chromatin is composed of DNA and protein in a nearly 1:1 ratio. In human cells, the DNA portion is comprised of approximately 4 billion base pairs in 23 pairs of chromosomes. The protein portion is comprised of primarily histone octamers along with more specialized proteins that stabilize specific structures such as heterochromatin or telomeres.[2,3] Even in its decondensed state, chromatin is far from a disorganized "bowl of spaghetti", with each chromosome occupying a distinct territory within the nucleus.[2] Furthermore, subregions within chromatin organize in such a way as to bring together genes that tend to be expressed at the same time called Transcriptionally Associated Domains (TADs) to increase the efficiency of gene expression.[2] The smallest structure that can reasonably be called chromatin, as opposed to DNA or a protein, is the nucleosome. Nucleosomes consist of DNA wrapped around a histone octamer which is composed of two each of the four histone protein archetypes, H2A, H2B, H3, and H4.[10] H1, conspicuously missing from the list, is a linker protein that connects nucleosomes to each other and is one of the defining features of heterochromatin.[10]

The histones in nucleosomes may be modified in two main ways to alter the structure, organization, and function of the chromatin. The first way that histones can be modified is by being swapped out for a variant of the same archetype, for instance H2A for H2AX or H3 for H3.3.[11,12] Some variants are only found in a particular cell type such as H2B.1 being found primarily in germline cells.[13,14] The second way that histones can be modified is by the

deposition of post-translational modifications (PTMs) onto a specific residue usually on one of the histone tails.[1,15,16,17] The most common of these PTMs are methylation, acetylation, and phosphorylation.[16] In general, methylation (i.e., H3K9me3) tends to cause the DNA to wind tighter around the histones condensing the chromatin and silencing transcription, but exceptions exist in which a methylation results in the opposite effect (i.e., H3K4me3).[18,19,20] Likewise, acetylation (i.e., H3K9Ac) tends to decondense the chromatin because the repelling negative charges of the acetyl group and the DNA backbone cause the DNA to unwind from the histones allowing greater access by transcription machinery.[21,22] Phosphorylation usually signals for the binding of certain proteins to the DNA.[12] In the case of γH2AX (phosphorylation of Ser139 on H2AX), these proteins are repair factors because γH2AX is deposited both up- and downstream of double strand breaks.[12] Chromatin is generally recognized as falling into one of two categories: heterochromatin or euchromatin. Recently, however, the actual structure of chromatin has been shown to be more of a continuum between these two poles and not specifically one or the other.[23] Even so, a region with a high density of H1 linkers and H3K9me3 marks would still accurately be described as heterochromatin, and a region with a high density of H3K9Ac marks would still accurately be described as euchromatin.

## Chromatin Mechanics

Chromatin generally acts as a fractally organized viscoelastic polymeric network.[24] However, because molecular machines such as helicases, polymerases, and motor proteins are near constantly exerting force upon chromatin, it is not always possible to simply model chromatin motion with a power law.[25,26] The molecular machines involved in Replication or Transcription exert direct force upon the chromatin because they are bound directly.[27,28]

Helicases generate twisting strain ahead of replication forks, which is then relieved by topoisomerases.[28,29] Polymerases move along the DNA itself like a tram on a monorail.[27] The average material properties of the chromatin network are altered by chromatin remodeling proteins such as histone deacetylases (HDACs) and Histone Acetyl Transferases (HATs).[30] HDACs lead to tighter winding of nucleosomes and HATs lead to more loosely wound nucleosomes.[30] Other molecular machines pull on chromatin indirectly through structural connections that link chromatin to the rest of the cell and its environment.[5] Chromatin is mechanically linked to the rest of the cell as it is bound to lamins that make up the nucleoskeleton which are in turn bound to the LINC complex which in turn connects to the cytoskeleton in various ways.[3,31] Furthermore, the chromatin also has a mechanical tether to the cell's exterior environment since the cytoskeleton is linked to the extracellular matrix through focal adhesions.[32] As a consequence, chromatin is constantly receiving both internal and external mechanical stimuli that may in turn alter gene expression. Under normal circumstances chromatin is organized in such a way that the synergy between chemical and mechanical stimuli leads to changes in gene expression that facilitate appropriate responses to these stimuli, an example of which is discussed in Chapter VI.

## Advantages of Investigating Phenomena via Mechanics

There are a multitude of biological processes running in parallel that could potentially affect any particular biological phenomenon. To determine the extent to which each of these processes contribute to the phenomenon of interest requires a battery of tests and controls that can be time-consuming and expensive and often do not contribute directly to testing the central hypothesis. Measuring the mechanical properties of the system in question can integrate all of

the individual contributions of each of these processes and provide data that speak to the validity of the hypothesis much more efficiently and cheaply.

Investigation of the mechanical microenvironment of a particularly complex or mysterious cellular phenomenon may also provide insight into the most likely contributors to said phenomenon. Understanding how the mechanical microenvironment is changed from before to after can help narrow down the culprit to proteins of interest capable of facilitating that change. This is the primary usefulness of the conclusions drawn in Chapters III, IV, and V.

## Sensors from IntraNuclear Kinetics (SINK)

Sensors from IntraNuclear Kinetics, or SINK, is a method of studying cellular mechanics that leverages the mechanical interconnectedness of chromatin to measure the effects of a variety of stimuli on the mobility of chromatin.[8] Knowing how chromatin is mechanically linked to other structures and the proteins that cause chromatin mobility to change in the observed manners allows for inferences to be made based upon SINK data as to the mechanism of the mobility changes.

Briefly, SINK is a particle tracking method that relies upon fluorescence microscopy. Chromatin bound proteins or DNA itself is labelled with any of a variety of fluorescent probes. Fluorescent stains or fluorescently tagged proteins, either transiently overexpressed or stably transduced, may be used. Live-cell imaging on one or more fluorescent channels is performed by taking images at regular intervals for a specified length of time starting either before, during, or after the stimulus of interest. Images are processed to crop individual nuclei, remove translational and rotational motion of the nuclei themselves (so as to track only motion of particles within the nuclei), and to calibrate for background noise in the fluorescent signal. Using

statistical algorithms individual particles are tracked and only tracks in which the particles persist through all frames in the sequence are retained. Location data from each particle is used to calculate the Mean Squared Displacement (MSD) of each particle for each Lag Time and these values are ensemble averaged and outliers removed. The MSDs may then be compared from experiments run before, during, or after a certain process, between different cell types undergoing the same stimulus, or between the same cell-type undergoing different stimuli. In many circumstances this is the final data gleaned from the SINK method, but, if certain assumptions hold, then the further step of fitting the MSD data to a power law may yield additional data. The SINK method is described in detail in Chapter II.

## Wide Range of Applications for SINK

SINK is a very robust method, useful in a variety of situations. Chromatin motion can be measured in a wide range of specificity, from a single locus to certain domains to the entire network. Any chromatin-bound protein of interest that can be fluorescently labeled may be tracked, and any cell type resilient enough to survive time-lapse fluorescent imaging may be studied.

### Site-specific damage foci mobility

Chapter III will focus on a project investigating how chromatin mobility changes after damage is induced by reactive oxygen and compare the response of heterochromatic regions to euchromatic regions. The measurement of chromatin mobility in this project was site-specific as only a single particle was tracked per cell because the fluorescently labeled probes only bound to

a specific sequence within the genome. Chapter III is a reprint of work published in Scientific Reports in December of 2018.[9]

**Subtle global mobility changes after drug treatment**

Chapter IV will focus on a project investigating chromatin mobility changes in healthy and malignant breast epithelial cells after treatment with the chemotherapy drug cisplatin. The measurement of chromatin mobility in this project was throughout the nucleus, as a fairly ubiquitous transcription factor was used as the fluorescently tagged chromatin bound probe. Chapter IV is a preprint of work that is being prepared for publication soon.

**Gross global reorganization after viral infection**

Chapter V will focus on a project investigating whether gross chromatin rearrangement during Herpes Simplex Virus 1 infection is primarily a mechanical process driven by overcrowding in the nucleus from the production of virions or a biological process driven by a chromatin remodeling pathway (or pathways) being activated by the invading virus. The measurement of chromatin mobility in this project was generalized as much as possible to track all regions of chromatin so data would not be biased toward either hetero- or euchromatin. Chapter V is a preprint of work that is being prepared for publication.

**Active damage prevention**

Chapter VI will focus on a project done in collaboration with the Wickstrom Lab at the University of Helsinki studying cells' ability to rearrange both their cytoskeleton and chromatin structure to prevent DNA damage induced by mechanical stress.[33] The measurement of

chromatin mobility was done at specific structures (telomeres) that are dispersed throughout the nucleus giving a fairly generalized view of the motion of the entire network. Unique in this project was the length of time that the experiments were run, and the intervals used between images. While the Dahl Lab has a standard experiment time length and a standard length of interval between images, SINK is a flexible enough method that these can be altered to fit different applications. Chapter VI is a summary of work focusing on this author's contribution to the work that was published in Cell in May of 2020.[33]

## References


1. Felsenfeld G. & Groudine M. Controlling the double helix. *Nature*. **421**, 448-453 (2003).
2. Fraser J., Williamson I., Bickmore W. A., & Dosie J. An Overview of Genome Organization and How We Got There: from FISH to Hi-C. *Microbiology and Molecular Biology Reviews*. **79**, 347-372 (2015).
3. Kaminski A., Fedorchak G. R., & Lammerding J. The cellular mastermind(?) – Mechanotransduction and the nucleus. *Prog Mol Biol Transl Sci*. **126**, 157-203 (2014).
4. Booth-Gauthier E. A., Alcoster T. A., Yang G. & Dahl K. N. Force-induced changes in subnuclear movement and rheology. *Biophys. J.* **103**, 2423-2431 (2012).
5. Spagnol S. T. & Dahl K. N. Active cytoskeletal force and chromatin condensation independently modulate intranuclear network fluctuations. *Int. Bio.* **6**, 523-531 (2014).
6. Booth E. A., Spagnol S. T., Alcoster T. A., & Dahl K. N. Nuclear stiffening and chromatin softening with progerin expression leads to an attenuated nuclear response to force. *Soft Matter*. 1-7 (2015).
7. Armiger T. J., Spagnol S. T., & Dahl K. N. Nuclear mechanical resilience but not stiffness is modulated by αII-spectrin. *Journal of Biomechanics*. **8**, 49-55 (2016).
8. Armiger T. J., Lampi M. C., Reinhart-King C. A., & Dahl K. N. Determining mechanical features of modulated epithelial monolayers using subnuclear particle tracking. *Journal of Cell Science*. **131**, 1-6 (2018).
9. Whitefield D. B., Spagnol S. T., Armiger T. J., Lan L., & Dahl K. N. Quantifying site-specific chromatin mechanics and DNA damage response. *Scientific Reports*. **8**, 1-9 (2018).
10. Luger K., Mader A. W., Richmond R. K., Sargent D. F., & Richmond T. J. Crystal structure of the nucleosome core particle at 2.8A resolution. *Nature*. **389**, 251-260 (1997).
11. Jang C., Shibata Y., Starmer J., Yee D., & Magnuson T. Histone H3.3 maintains genome integrity during mammalian development. *Genes & Development*. **29**, 1377-1392 (2015).

12. Kleiner R. E., Verma P., Molloy K. R., Chait B.T. & Kapoor T. M. Chemical proteomics reveals a γH2AX-53BP1 interaction in the DNA damage response. *Nat. Chem. Biol.* **11**, 807-814 (2015).
13. Li A., Maffey A. H., Abbott W. D., e Silva N. C., Prunell A., Siino J., Churikov D., Zalensky A. O., & Ausio J. Characterization of Nucleosomes Consisting of the Human Testis/Sperm-Specific Histone H2B Variant (hTSH2B). *Biochemistry*. **44**, 2529-2535 (2004).
14. Talbert P. B. et al. A unified phylogeny-based nomenclature for histone variants. *Epigenetics & Chromatin*. **5**, 1-19 (2012).
15. Allfrey V. G., Faulkner R., & Mirsky A. E. Acetylation and Methylation of Histones and their Possible Role in the Regulation of RNA Synthesis. *PNAS*. **51**, 786-794 (1964).
16. Cosgrove M. S., Boeke J. D., & Wolberger C. Regulated nucleosome mobility and the histone code. *Nature Structural & Molecular Biology*. **11**, 1037-1043 (2004).
17. Fenley A. T., Adams D. A., & Onufriev A. V. Charge State of the Globular Histone Core Controls Stability of the Nucleosome. *Biophysical Journal*. **99**, 1577-1585 (2010).
18. Barski A., Cuddapah S., Cui K., Roh T., Schones D. E., Wang Z., Wei G., Chepelev I., & Zhao K. High-Resolution Profiling of Histone Methylations in the Human Genome. *Cell*. **129**, 823-837 (2007).
19. Koch C. M. et al. The landscape of histone modifications across 1% of the human genome in five human cell lines. *Genome Research*. **17**, 691-707 (2007).
20. Rosenfeld J. A., Wang Z., Schones D. E., Zhao K., DeSalle R., & Zhang M. Q. Determination of enriched histone modifications in non-genic portions of the human genome. *BMC Genomics*. **10**, 1-11 (2009).
21. Creyghton M. P. et al. Histone H3K27ac separates active from poised enhancers and predicts developmental state. *PNAS*. **107**, 21931-21936 (2010).
22. Pradeepa M. M., Grimes G. R., Kumar Y., Olley G., Taylor G. C. A., Schneider R., & Bickmore W. A. Histone H3 globular domain acetylation identifies a new class of enhancers. *Nature Genetics* **48**, 681-688 (2016).
23. Ou H. D. *et al*. ChromEMT: visualizing 3D chromatin structure and compaction in interphase and mitotic cells. *Science* **357**, 1-13 (2017).
24. Dahl K. N., Engler A. J., Pajerowski J. D., & Discher D. E. Power-Law Rheology of Isolated Nuclei with Deformation Mapping of Nuclear Substructures. *Biophysical Journal*. **89**, 2855-2864 (2005).
25. Hameed F. M., Rao M., & Shivashankar G. V. Dynamics of Passive and Active Particles in the Cell Nucleus. *PlosOne*. **7**, 1-11 (2012).
26. Smith K., Griffin B., Byrd H., McKintosh F. C., & Kilfoil M. L. Nonthermal Fluctuations and Mechanics of the Active Cell Nucleus. *Biophysics*. 1-5 (2013).
27. Cramer P. et al. Structure of Eukaryotic RNA Polymerases. *Annual Review of Biophysics*. **37**, 337-352 (2008).
28. Patel S. S. & Donmez I. Mechanisms of Helicases. *Journal of Biological Chemistry*. **281**, 18265-18268 (2006).
29. Champoux J. J. DNA Topoisomerases: Structure, Foundations, and Mechanism. *Annual Review of Biochemistry*. **70**, 369-413 (2001).
30. Swygert S. G. & Peterson C. L. Chromatin dynamics: Interplay between remodeling enzymes and histone modifications. *Biochim Biophys Acta*. **1839**, 728-736 (2014).

31. Szczesny S. E. & Mauck R. L. The Nuclear Option: Evidence Implicating the Cell Nucleus in Mechanotransduction. *Journal of Biomechanical Engineering*. **139**, 1-16 (2017).
32. Sun Z., Guo S. S., & Fassler R. Integrin-mediated mechanotransduction. *Journal of Cell Biology*. **215**, 445-456 (2016).
33. Nava et al. Heterochromatin-Driven Nuclear Softening Protects the Genome against Mechanical Stress-Induced Damage. *Cell*. **181**, 800-817 (2020).

# Chapter II

## Methods

### Introduction

The use of particle tracking techniques to measure the mechanical properties of soft materials can be traced back to the work of the Weitz lab.[1] Measurement of the mechanical properties of chromatin in particular is made possible by particle tracking techniques provided that the particles being tracked are bound directly to the chromatin. This is the idea behind Sensors from IntraNuclear Kinetics (SINK), the particle tracking technique used for every major project within this thesis.[2,3] SINK is a single particle tracking technique taking advantage of fluorescently tagged probes, such as UBF1 or TRF1, that bind directly to chromatin in discrete foci. Cells are imaged at regular intervals for a set amount of time, usually every 3 minutes for 1 hour. These images are processed using ImageJ and MATLAB to align multiple channels, subtract motion of the nucleus itself (so that only movement within the nucleus is measured), and calibrate for background noise. Particles are identified and tracked through every frame of the movie generated. Only particles that appear in every frame are tracked, the rest are removed from analysis. Mean Squared Displacements (MSDs) are calculated from the location data in these tracks. In general, a higher MSD indicates more mobile chromatin.[2,3,4,5,6,7,8] If MSD plots seem to be scale invariant, that is, the plot appears to be linear in loglog coordinates, then the MSD may be fit to a power law ($MSD(\tau) = D_{eff} * \tau^{\beta}$) to extract more information, as seen in Booth-Gauthier, Biophysical Journal, 2012; Spagnol, Integrative Biology, 2014; Booth, Soft Matter, 2015; and Armiger, Journal of Cell Science, 2018.[4,5,6,8] If MSD plots vary with timescale, then certain assumptions, discussed later in the chapter do not hold and data cannot be

fit to a power law in a meaningful way, as seen in Whitefield, Scientific Reports, 2018; Nava, Cell, 2020; and Armiger, Journal of Biomechanics, 2016. [2,3,7] The coefficient, $D_{eff}$, has previously been shown to be related to chromatin compliance and condensation state, i.e. how tightly or loosely wound the DNA is around histones in each nucleosome.[5,6] The lower the $D_{eff}$, the more condensed the chromatin is. The exponent, β, has previously been shown to be related to force propagation throughout the chromatin network.[5,6] The higher the β, the greater the force acting through the chromatin. In simplified terms, a translation of the MSD plot in the y-direction indicates a change in chromatin compliance or condensation between two conditions, and a change in the apparent slope of the MSD plot indicates a change in force generation between two conditions.

## Microscopy

The first step in the microscopy portion of SINK is preparing a sample of cells to be imaged. Cells of interest are usually grown to confluency or near confluency in appropriate imaging dishes, most commonly, Ibidi 35mm μ-dishes. Cells are not required to be confluent, however. Experiments with isolated single cells or cells at the edge of a wound in a scratch assay may also be imaged and analyzed. Although, that the cells are adherent to the dish is a requirement of the SINK method. The next consideration to be made while preparing the sample of cells to be imaged is the chromatin bound fluorescent probe. Stably transduced cells are ideally already prepared for imaging. However, cells requiring staining (with, for instance, Hoechst 33342) or transient transfection (with, for instance, appropriate plasmids and Lipofectamine 3000) should be stained or transfected at this point. Any drug treatment, mechanical manipulation, viral infection, or any other experimental stimulus being tested should

be completed (in the case of one-time stimuli) or initiated (in the case of a continuous stimulus) before imaging begins.

The next step is to prepare the microscope for the SINK experiment. Experiments are usually performed on microscopes with climate control chambers surrounding the stage that regulate temperature, $CO^2$ content, and humidity as these experiments are meant to be performed on living cells. The only exceptions are experiments in which one of those variables is changed as the experimental stimulus to the cells. The particular apparatus used for most experiments described in this work consists of a widefield fluorescence microscope (DMI6000, Leica, Buffalo Grove, IL – 63x, 1.4 NA, inverted oil immersion objective). Additionally, this microscope is equipped with a live-cell imaging chamber built around the stage outfitted with a heater and thermostat to keep the chamber at 37°C and a humidifier containing MilliQ water that has a steady flow of 5% $CO^2$ being bubbled through the reservoir to simultaneously provide $CO^2$ and humidity. The best practice for running a SINK experiment is to turn on the heater 24 hours beforehand so that not only is the air temperature at 37°C, but all surfaces inside the live-cell imaging chamber are equilibrated to 37°C as well. A stable temperature prevents focal drift while imaging. Flow of $CO_2$ may be initiated just prior to the beginning of the experiment. Typical SINK experiments are run using an inverted 63x oil immersion objective. Other settings may be used as long as the pixel:micron ratio is known for each experiment.

Once the sample of cells to be analyzed and the microscope are prepared for an experiment, the imaging dish containing the cells of interest may be placed on the stage and brought into contact with the oil on the objective. Various imaging channels are then set up in the microscope software including a brightfield channel (to verify that cells do not die or divide during or soon after the experiment) and fluorescent channels appropriate to the experimental

setup. As many fluorescent channels as is practical may be used depending on the fluorescently tagged chromatin bound proteins in the sample cells, the color cubes on the microscope, and the overlap of the spectra of the fluorescent probes. Although, there are typically only 2 or 3 fluorescent channels per experiment. Illumination intensity and duration settings should be adjusted to find the optimal balance between maximizing fluorescence so that particles are visible (trackable) and minimizing phototoxicity and photobleaching so that the cells do not die and the fluorescent probes are not photobleached before the experiment ends. To maximize the data from each experiment it is useful to set up multiple imaging fields of view, or positions, typically 8-12. Another way to maximize the data gleaned from each experiment, this time by preventing data loss due to focal drift, is to program the microscope to take images at multiple z-heights (focus heights) per field of view, typically 5. These are usually defined 1-2 μm apart. The automated time lapse imaging program should also be set up. Most experiments in this work were programed to take images of every position and z-height every 3 minutes for 1 hour resulting in a 21 frame 'movie', but SINK is flexible enough to allow for a wide range of intervals and overall experiment lengths, as demonstrated in Chapter VI.

## Preprocessing

The next phase of SINK is the fairly straight forward process of preprocessing the images. First, the microscope files are exported as a file type that is ideally relatively easy to work with in ImageJ and that retains the highest amount of data about the images, usually a .tiff file. The images are then sorted into a well-organized (as defined by the researcher) file architecture. Finally, the images are cropped so that movies for each individual nucleus can be further sorted into the well-organized (as defined by the researcher) file architecture.

## Alignment and Calibration

Once the movies for the individual nuclei have been sorted, they are processed through statistical algorithms that clean up the image data into something useful. If multiple fluorescent channels exist in a particular experiment, then these may be aligned to each other, meaning that any rotation or translation of an image file in the first channel is applied to the corresponding image files at the same time point in the subsequent channels. The translational and rotational motion of each nucleus is subtracted so that when the particles within the nucleus are tracked only the motion of the particles are measured and not the motion of the nucleus itself. Lastly, the images are calibrated for background noise so that a high background does not distort the data.

## Mean Squared Displacement

Finally, particles are identified, and their position data is tracked through each frame of the movie. From this data, the Mean Squared Displacement (MSD) of the particle can be calculated at each value of Lag Time, $\tau$. Particles are identified by statistical algorithms as the centroid of regions with a higher intensity of fluorescence signal. Another statistical algorithm performs a search for the new location of each particle in the next frame in a predefined radius around the location of each particle from the previous frame. If no particle can be found within that circle, that track is removed from the analysis as only tracks that persist through all frames of the movie are recorded. Using the location data of each particle for every time point, the MSD is calculated using Equation 1, where $\tau$ is Lag Time.

$$MSD(\tau) = \langle (x_{t+\tau} - x_t)^2 + (y_{t+\tau} - y_t)^2 \rangle \qquad (1)$$

Lag Time requires further explanation as it is more similar to a frequency than actual time. The Mean in MSD is the average of the $\{\text{displacement}\}^2$ of every time interval of the size

of Lag Time. Specifically, MSD($\tau$=3 minutes) is not the average {displacement}$^2$ that every particle traveled over the first 3 minutes of the experiment, but rather the average {displacement}$^2$ that a particular particle traveled during every 3 minute interval of the experiment, whether the first 3 minutes or the last 3 minutes. For a typical 21 frame movie, every MSD($\tau$=3 minutes) is the average of 20 data points, every MSD($\tau$=6 minutes) is the average of 19 data points, and so on until MSD($\tau$=60 minutes) is no longer technically a Mean because there is only 1 interval of 60 minutes in an hour long experiment. Obviously, from this fact, it is easy to see that uncertainty in MSD increases as Lag Time increases. It is therefore necessary to analyze many cells, preferably with many trackable particles each, to have confidence in the trends at later Lag Times.

## Curve Fitting

If certain assumptions are met, the MSD data can be fit to a power law to extract even more data from SINK experiments. This power law is of the form of Equation 2 below where $\tau$ is Lag Time, $D_{eff}$ is related to chromatin condensation, and $\beta$ is related to force propagation.[5,6]

$$MSD(\tau) = D_{eff} * \tau^{\beta} \quad (2)$$

The assumptions that must be met are that chromatin mobility is timescale invariant and chromatin motion is not erratic. Timescale invariant means that $\beta$ is independent of choice of $\tau_0$.[9] In this case $\tau_0$ is 3 minutes. For Equation 2 to hold, any selection of $\tau_0$ should lead to the same calculated value of $\beta$. For the motion of chromatin in most adhered cells this assumption holds true unless a particular cellular process is actively remodeling the nuclear architecture, which is primarily due to the fractal organization of chromatin.[9,10] For chromatin motion to not be

considered erratic, β must be constant. In practical terms, this means that the MSD plots must appear linear in logarithmic coordinates.

Spagnol, Integrative Biology, 2014 showed the physical meaning of $D_{eff}$ and β using SINK. $D_{eff}$ was increased as decondensation increased while β remained unchanged in a series of experiments involving two drugs, Daunomycin and Trichostatin A, both of which cause global chromatin decondensation, albeit through differing mechanisms.[5] Similarly in another series of experiments in which the nucleus was either mechanically decoupled from the cytoskeleton or myosin motors were inhibited, β was affected by the change in forces acting upon the nucleus while $D_{eff}$ was not.[5]

## References


1. Mason T. G. & Weitz D. A. Optical Measurements of Frequency-Dependent Linear Viscoelastic Moduli of Complex Fluids. *Physical Review Letters*. **74**, 1250-1253 (1995).
2. Whitefield D. B., Spagnol S. T., Armiger T. J., Lan L., & Dahl K. N. Quantifying site-specific chromatin mechanics and DNA damage response. *Scientific Reports*. **8**, 1-9 (2018).
3. Nava et al. Heterochromatin-Driven Nuclear Softening Protects the Genome against Mechanical Stress-Induced Damage. *Cell*. **181**, 800-817 (2020).
4. Booth-Gauthier E. A., Alcoster T. A., Yang G. & Dahl K. N. Force-induced changes in subnuclear movement and rheology. *Biophys. J.* **103**, 2423-2431 (2012).
5. Spagnol S. T. & Dahl K. N. Active cytoskeletal force and chromatin condensation independently modulate intranuclear network fluctuations. *Int. Bio.* **6**, 523-531 (2014).
6. Booth E. A., Spagnol S. T., Alcoster T. A., & Dahl K. N. Nuclear stiffening and chromatin softening with progerin expression leads to an attenuated nuclear response to force. *Soft Matter*. 1-7 (2015).
7. Armiger T. J., Spagnol S. T., & Dahl K. N. Nuclear mechanical resilience but not stiffness is modulated by αII-spectrin. *Journal of Biomechanics*. **8**, 49-55 (2016).
8. Armiger T. J., Lampi M. C., Reinhart-King C. A., & Dahl K. N. Determining mechanical features of modulated epithelial monolayers using subnuclear particle tracking. *Journal of Cell Science*. **131**, 1-6 (2018).
9. Kollmannsberger P. & Fabry B. Linear and Nonlinear Rheology of Living Cells. *Annu Rev Mater Res*. **41**, 75-97 (2011).
10. Dahl K. N., Engler A. J., Pajerowski J. D., & Discher D. E. Power-Law Rheology of Isolated Nuclei with Deformation Mapping of Nuclear Substructures. *Biophysical Journal*. **89**, 2855-2864 (2005).

# Chapter III

## Local Chromatin Mechanics of Site Specific DNA Damage

### Introduction

The human genome is four gigabases of double stranded DNA wound onto histones to form chromatin with loose spatial organization inside the nucleus[1]. The rheological consequences of this highly entangled polymeric system are impacted by numerous factors including chromatin density and molecular motors[2,3]. Recently, it has been shown that chromatin inside of cells is less binary in its higher-order structure than thought previously: there are a continuum of condensation states with most chromatin existing as 5-24 nm diameter chromatin fibers[4] rather than more rigidly defined heterochromatin and euchromatin. Thus, to examine the dynamics of chromatin, we employ a system utilizing a human osteosarcoma cell line with a stably incorporated cassette of 96 Tetracycline Response Elements (TREs), named U2OS-TRE, incorporated at a site of heterochromatin near the centromere of the X-chromosome previously described in Lan et al., 2014[5] and Wei et al., 2015[6]. TREs are sequences of DNA that allow for control of gene expression through their binding of either Transcription Activator (TA) or Tetracycline Repressor (TetR) proteins[5,6]. TA binding to the TRE leads to transcriptional activation and concomitant chromatin decondensation, and TetR binding to the TRE reinforces transcriptional repression and chromatin condensation[5,6]. While this allows the spatial advantage of examining specific chromatin territories, this method introduces challenges of data analysis from the tracking of a single point within a living cell. We utilize multichannel registration particle tracking algorithms to process images and remove rigid body nuclear motion to track single particle loci, allowing for fiducial image stacks of persistent sub-nuclear motion[2,7]. We

find that transcriptionally active regions exhibit chromatin dynamics equivalent to bulk chromatin (as measured by chromatin probes bound inside nucleoli and at telomeres) and transcriptionally repressed regions have reduced mobility consistent with their tight condensation state.

We further explore the impact of DNA damage at different loci by inducing DNA double strand breaks (DSBs) using the KillerRed (KR) fluorescent protein bound to TA and TetR, respectively. KR releases superoxide upon green light activation and is known to induce DSBs, among other DNA lesions, locally at the sites of expression[5,6]. DNA damage influences a variety of nuclear functions related to gene expression, replication, and regulation. Many of the molecular factors required for repair of DSBs have been investigated through *in vitro* protein-protein and protein-nucleic acid assays[8], imaging at the sites of damage in cells modulated through RNAi[9], and studies of disease models[10].

Some recent studies have begun to examine the chromatin dynamics of DNA damage and repair. As expected, the nucleosome must be reorganized for DNA to be spliced back together and histones are displaced in response to DSBs[11,12]. Global chromatin mobility within the nucleus after DNA damage has also been studied using particle tracking to investigate the impact of repair proteins[13,14,15] or to consider different repair pathways[16,17]. Here, we investigate DNA damage within distinct chromatin regions while also comparing chromatin mobility within the rest of the nucleus. We observe that DSBs in transcriptionally repressed regions of chromatin, which typically have reduced mobility relative to bulk or transcriptionally active chromatin, exhibit enhanced dynamics more akin to bulk chromatin following DNA damage induction. Transcriptionally active regions, by contrast, undergo time-dependent changes following DNA damage culminating in chromatin relaxation and reduced force propagation from motor protein

activity experienced at these sites, consistent with a physical decoupling of the chromatin network. The resulting effect decreases the probability of large length scale (length scales that make translocations likely) chromatin motion at long timescales, thereby reducing the potential for improper repair and translocations.

## Results

### Measuring chromatin dynamics by bound probes

We measure chromatin dynamics inside of nuclei by tracking fluorescently tagged, exogenously expressed, chromatin bound proteins. We have previously demonstrated that ensemble chromatin dynamics on long time scales (minutes) are independent of the chromatin-associated probes. Specifically, in previous work GFP-Fibrillarin and Hoechst 33342 showed indistinguishable MSDs[2] and GFP-Fibrillarin, a nucleolar protein, and GFP-UBF1, a ubiquitous transcription factor, were similar to one another; different cell types showed different magnitudes of MSD but a consistency between chromatin-bound probes[7,18]. Theoretically, the mechanics of a viscoelastic polymer solution can be determined from tracking any bound particle in the solution. Here, we track bulk chromatin movements of intranuclear proteins in U2OS human osteosarcoma cells transfected with fibrillarin (GFP-Fibrillarin) or telomeric repeat-binding factor 1 (RFP-TRF1) (Figure 3.1A, B). Fibrillarin was chosen because it binds to dense nucleolar regions scattered throughout the nucleus and probes "interstitial" chromatin - chromatin not in close proximity to the end of a chromosome. Conversely, TRF1 was chosen because it specifically binds to telomeres in the nucleus[13] and probes individual "terminal" chromatin with distinct speckles, allowing for tracking with lower background. Thus, fibrillarin and TRF1 are spatially (Figures 3.1A versus 3.1B) and functionally distinct chromatin moieties. After

processing the images to remove rigid body motion of the nucleus and finding centroids of persistent particles, we averaged the mean squared displacement (MSD) of the chromatin bound proteins and plotted these movements versus lag time (Supplemental Figure 1). For more detailed description of image processing, see the Materials and Methods section or Supplemental Figure 1. Similar to our other studies, MSDs of GFP-Fibrillarin and RFP-TRF1 are statistically indistinguishable in U2OS cells (Figure 3.1C) despite their differential spatial distribution and functional role within the nucleus. We suggest that this similarity in MSD from particle tracking of disparate chromatin-bound probes is consistent with our measurements at these timescales being indicative of ensemble chromatin dynamics of a dense, entangled polymer network. Other work has similarly demonstrated physical mechanisms driving coherent, micrometer-scale chromatin dynamics at short time scales that likely facilitates the physical uniformity of these

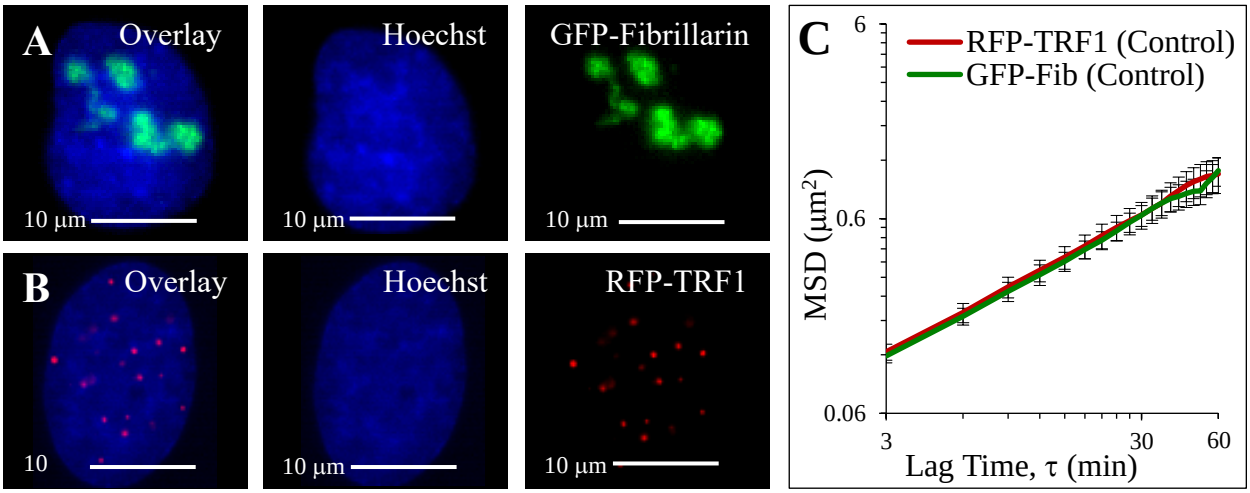


ensemble chromatin dynamics at our time scales[3].

***Figure 3.1: Bulk chromatin motion measurements are independent of bound probe.*** *Nuclei in both cases are stained with Hoechst 33342* ***A)*** *U2OS cell transfected with GFP-Fibrillarin showing localization of Fibrillarin within nucleoli.* ***B)*** *U2OS cell transfected with RFP-TRF1 showing TRF1 localization at telomeres.* ***C)*** *MSDs of RFP-TRF1 (n=17), in red, and GFP-Fibrillarin (n=13), in green, tracked in untreated control U2OS cells. Lines overlap each other*

*indicating that measurements of MSDs taken from different probes yield equivalent results. Error bars are SEM.*

**Tracking chromatin motion in transcriptionally active or transcriptionally repressed regions**

To investigate the distinct chromatin dynamics of transcriptionally active and repressed regions (as opposed to bulk chromatin dynamics) we tracked specific chromatin sites at which we could manipulate transcriptional activity. The effects of heterogeneities of sequences can be diminished with the system. U2OS-TRE has a stably incorporated array of TREs that could be targeted by TetR or TA (TetR+VP16) after transfection to manipulate of transcriptional activity and track motion as previously described[5,6]. To show that TA activates transcription we transfected U2OS-TRE cells with Transcription Activated mCherry (TA-mCh) and imaged Histone 3 acetylated at Lysine 9 (H3AcK9), a histone modification associated with transcriptionally active regions, by immunostaining (Figure 3.2A). Similarly, we transfected U2OS-TRE cells with Tetracycline Repressor mCherry (TetR-mCh) and immunostained Histone 3 dimethylated at Lysine 9 (H3DiMeK9), a histone modification that indicates transcriptionally repressed chromatin (Figure 3.2B). Additionally, we quantified baseline chromatin dynamics of the TRE array by tracking these regions in live human cell nuclei.

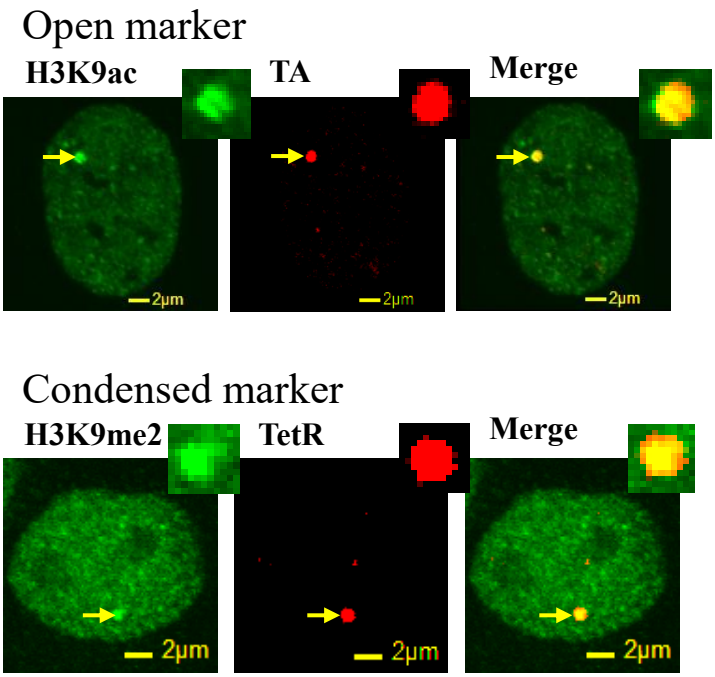


***Figure 3.2: Co-localization of TA and TetR loci with markers of euchromatin and heterochromatin markers, respectively.*** *Co-localization of TA-mCherry with AcH3K9 indicating that the TA motif localizes to regions of euchromatin, and co-localization of TetR-mCherry with DiMeK9H3 indicating that the TetR motif localizes to regions of heterochromatin.*

Cells were also co-transfected with GFP-Fibrillarin to visualize the bulk chromatin motion not associated with the TRE array. Our results demonstrate the chromatin dynamics of the bulk network, measured by cotransfected GFP-Fibrillarin and transcriptionally active regions (TA-mCh) were indistinguishable (Figure 3.3A). By contrast, transcriptionally repressed chromatin regions (TetR-mCh) exhibited a significant decrease in mobility from transcriptionally active regions (TA-mCh) and the bulk chromatin motion (Figure 3.3B) demonstrating that repressed regions are less mobile than transcriptionally active and bulk chromatin motion.

**Tracking DNA damage sites with KillerRed labeled tracer proteins**

Since there was a dramatic difference in chromatin dynamics between the transcriptionally repressed regions of chromatin relative to bulk chromatin and transcriptionally active regions of the genome, we explored how DNA damage impacts chromatin dynamics at

these sites. To investigate this, we activated KillerRed labeled TA or TetR (in lieu of mCherry) with white light to induce DNA damage at these same TRE regions. Damage induced by TA-KR colocalizes with γH2AX and 53BP1 (Supplemental Figure 2 and previous studies[5]). Bulk chromatin and transcriptionally active sites had no detectable difference in MSD following KillerRed-induced DNA damage (Figure 3.3C). By contrast, chromatin dynamics at transcriptionally repressed (TetR-KR) sites were increased (from non-damaged baseline (TetR-mCh)) in response to KillerRed-induced DNA damage, now resulting in motion indistinguishable from transcriptionally active (TA-KR) and bulk chromatin (Figure 3.3D). This observation is consistent with previous work where DSB induction at condensed, transcriptionally repressed regions results in a transition to a more decondensed state[19], further indicating that site-specific damage also leads to differential local chromatin dynamics.

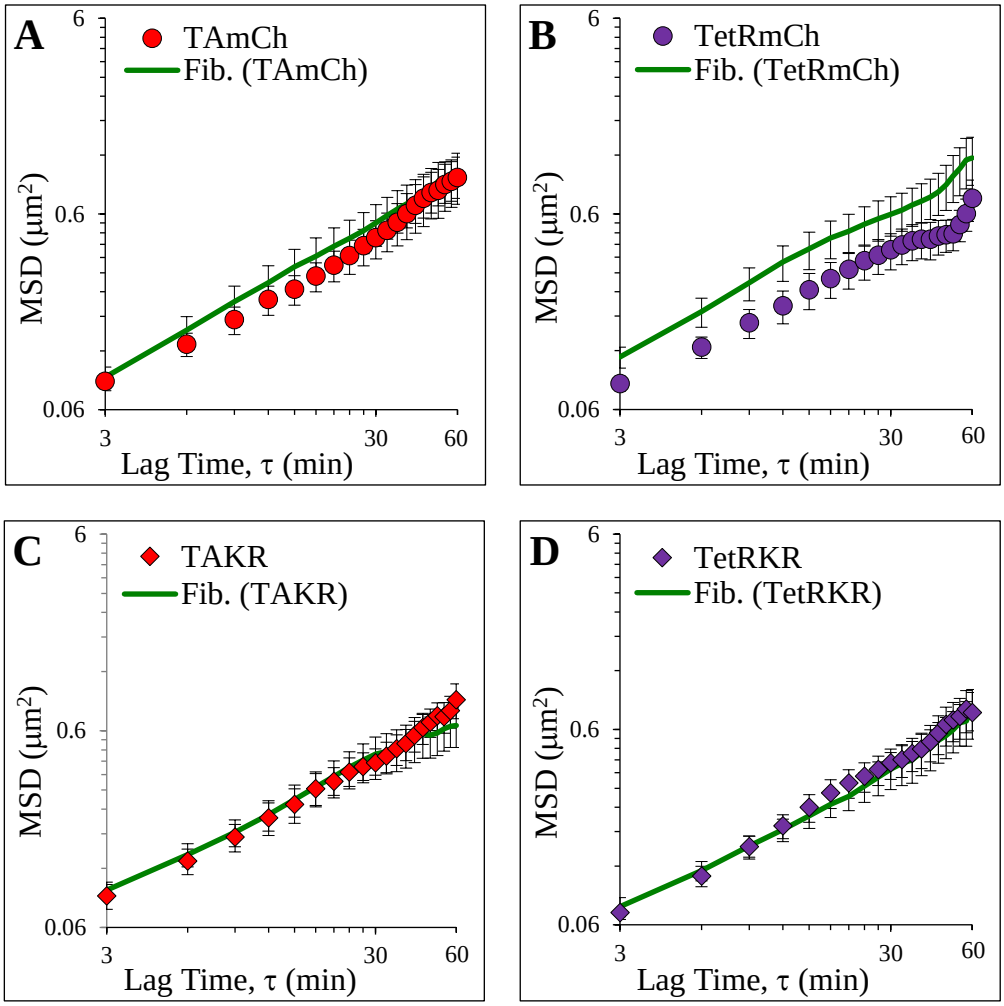


***Figure 3.3: MSDs comparing mobility of the bulk chromatin motion to the four tracers.*** *Bulk chromatin motion measured as cotransfected GFP-Fibrillarin.* ***A)*** *TA-mCherry (TA-mCh) denoted by red circles (n=34), cotransfected GFP-Fibrillarin (Fib. (TA-mCh)) denoted by green line (n=30),* ***B)*** *TetR-mCherry (TetR-mCh) denoted by purple circles (n=27), cotransfected GFP-Fibrillarin (Fib. (TetR-mCh)) denoted by green line (n=31),* ***C)*** *TA-KillerRed (TA-KR) denoted by red diamonds (n=20), cotransfected GFP-Fibrillarin (Fib. (TA-KR)) denoted by green line (n=25), and* ***D)*** *TetR-KillerRed (TetR-KR) denoted by purple diamonds (n=19), cotransfected GFP-Fibrillarin (Fib. (TetR-KR)) denoted by green line (n=21). Error bars are SEM.*

**Time dependence of chromatin dynamics**

Interestingly, DNA damage appeared to impact the chromatin dynamics of transcriptionally repressed, but not at transcriptionally active sites. Given that the majority of transcriptionally active sites are already decondensed for transcription activation, we considered that allowing additional time may change the chromatin dynamics[2]. We cotransfected cells with TA-KR and GFP Fibrillarin and induced damage as before, but for this experiment we measured chromatin dynamics after extended time (2 additional hours) post-damage (Figure 3.4A). Chromatin at damage foci 2 hours later had increased mobility compared to measurements early after damage, but similar mobility compared to measurements of 53BP1 foci in bleocin treated cells discussed in the next section (Figure 3.4B). Unlike other measurements of chromatin, this data showed skew at long lag times and suggesting large variability potentially associated with the presence of DNA lesions other than DSBs due to the high local concentration of ROS.

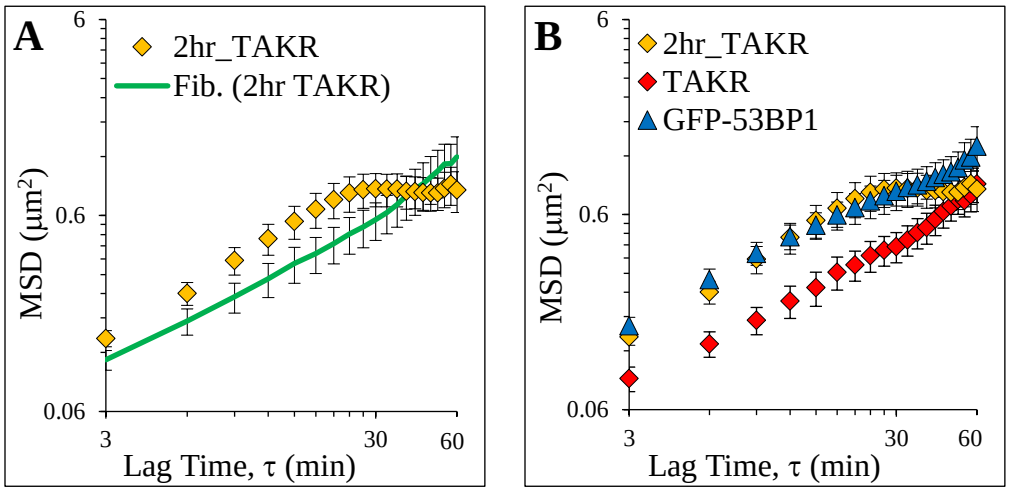


***Figure 3.4: Comparison MSDs showing temporal and global response of chromatin to DNA damage. A)*** *TA-KillerRed after 2 hours (2hr_TA-KR) denoted by orange diamonds (n=22), cotransfected GFP-Fibrillarin (Fib. (2hr TA-KR)) denoted by green line (n=26), and* ***B)*** *TA-KillerRed after 2 hours (2hr_TA-KR) again denoted by orange diamonds (n=22), TA-KillerRed*

*(TA-KR) denoted by red diamonds (n=20), and GFP-53BP1, denoted by blue triangles (n=12). Mobility is increased after 2 hours. 2hr_TA-KR displays dramatic skew at longer lag times. Error bars are SEM.*

**Effects of non-specific, nucleus-wide DNA damage**

To measure regions of the chromatin in response to non-specific, nucleus-wide DNA damage, we cotransfected U2OS cells with RFP-TRF1 as well as a protein that binds to double strand breaks: tumor suppressor p53-binding protein 1, GFP-53BP1[20]. We then treated these cells with bleocin for two hours to non-specifically induce nucleus-wide DSBs (Figure 3.5A). Following DNA damage induction, the undamaged chromatin sites (labeled with RFP-TRF1 or, in separate experiments, labeled solely with GFP-Fibrillarin following bleocin treatment) show similar MSD to chromatin dynamics of control untreated cells labeled by GFP-Fibrillarin or RFP-TRF1 (Supplemental Figure 3). Thus, global chromatin MSD appears to be unaffected by the bleocin treatment or fluorescent probe used. However, we observe enhanced chromatin movement in the regions associated with GFP-53BP1, a protein associated with the DNA damage response[21] (Figure 3.5B, triangles). While undamaged chromatin appears capable of maintaining the same behavior as control cells, the movements appear to be different in sites of DNA damage repair and shows increased chromatin movements on these time scales, similar to TA-KR after extended times (2 hours) but with increased certainty.

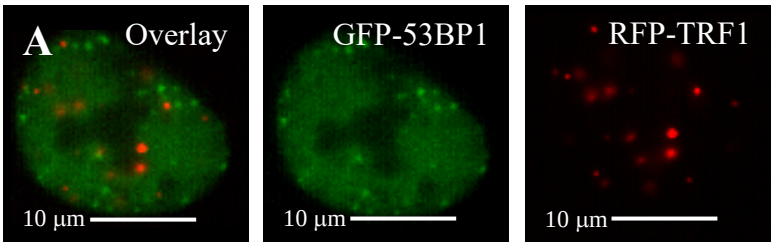


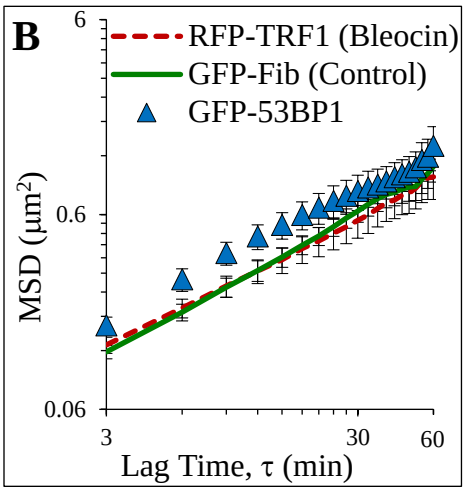


***Figure 3.5: MSDs showing decoupled chromatin dynamics induced by DNA damage. A)*** *U2OS cell treated with bleocin for 2 hours prior to imaging showing the localization patterns exhibited by GFP-53BP1 and RFP-TRF1.* ***B)*** *MSDs from RFP-TRF1 (n=18) in U2OS cells treated with bleocin, shown in red, and GFP-Fibrillarin (n=13) in untreated control U2OS cells, shown in green, showing similar mobility to each other despite global damage induction, but increased mobility in damage loci marked by GFP-53BP1 (n=12), shown as blue triangles. Error bars are SEM. GFP-53BP1 previously used in Figure 3.4B. GFP-Fibrillarin (Control) previously used in Figure 3.1C.*

## Discussion

The use of particle tracking allows for the characterization of the mechanical microenvironment of the nucleus. The U2OS-TRE system developed by Lan et al. 2014[5] allows for site-specific (in repressed or active chromatin) measurements of chromatin dynamics, as well as allowing for comparison to the bulk chromatin dynamics of the network. To this end, in this study we quantified chromatin dynamics at microenvironments of specific sites of transcriptionally repressed (TetR-mCherry) and transcriptionally active (TA-mCherry) chromatin, then compared these to the bulk chromatin motion (cotransfected GFP-Fibrillarin). This comparison revealed that transcriptionally active chromatin has similar chromatin dynamics to that of the bulk chromatin network. Transcriptionally repressed chromatin, however, displayed

reduced mobility compared to that of the bulk average. We previously showed the Hoechst 33342-rich regions, which are higher in heterochromatin content, showed no different mobility than other regions of the chromatin[2]. This is consistent with the idea that the genome is mostly a continuum of chromatin states rather than binary heterochromatin or euchromatin[4]. However, in this case we find a slightly lowered mobility for a singular region that is highly, structurally and functionally compacted.

Replacing mCherry tagged probes with KillerRed tagged probes allowed us to measure changes in mobility after damage had been induced. No significant change could be observed in the mobility of transcriptionally active regions after damage was induced on the order of minutes for a timescale under 2 hours. In transcriptionally repressed regions, however, the mobility increased after damage induction to match that of the bulk mobility of the chromatin network indicating that repressed regions of chromatin become more mobile in response to DNA damage. This observation fits well with previous observations of differential nuclear movements in response to DSBs in heterochromatin versus euchromatin (reviewed nicely in [22]). Recent work in the model *Drosophila* system with distinct heterochromatin and euchromatin regions has shown directionalized movement of heterochromatin after damage[23]. Analysis of our data for preferred directionality did not show any oriented movement despite changes in overall MSD speed (Supplemental Figure 4), but this difference could also be due to reduced overall movements compared to the *Drosophila* system. It is important to note that since the TRE array is incorporated into transcriptionally repressed regions, even if transcription has been activated by TA and a local region of decondensed chromatin has formed, there may be subtly distinct features displayed by the chromatin dynamics at this induced locus as compared to true endogenous gene expression. Nevertheless, our system provides valuable insight into site-

specific differences in chromatin dynamics between transcriptionally active and repressed regions following DNA damage. Previous studies have suggested alternate pathways of DNA damage repair: Homologous Recombination for active chromatin and Non-Homologous End Joining for repressed chromatin[16,17]. While this biophysical study does not consider repair pathways, we observe a relaxation of the repressed chromatin in response to DNA repair processes. This may suggest a minimal fluctuation state of the chromatin or local chromatin territory needed for access of repair factors, despite the pathway used.

We compared chromatin mobility early (microscope experimental setup requires approximately 45 minutes from the completion of damage induction) after ROS induced damage in open chromatin regions (TA-KR), after 2 hours (plus microscope setup) of ROS induced damage (2hr_TA-KR), and globally after 2 hours (plus microscope setup) of bleocin induced damage (bleocin with GFP-53BP1). The initial damage did not show increased mobility, but with increasing time chromatin mobility increased compared to the rest of the chromatin in the nucleus. This is an important consideration since the damaged regions are apparently mechanically decoupled from the rest of the chromatin meshwork. This is in contrast to our previous findings, recapitulated here in Figure 3.1, that chromatin mechanics can reliably be measured using any other bound probe in any other compartment within the nucleus (telomere, nucleolus, DNA, etc.)[24].

Previous studies using different imaging modalities and model systems have examined the temporal response to DNA damage and repair. Collectively previous research suggests chromatin decondensation in the first 90 seconds post-damage and recondensation 30 minutes after damage, in some cases to a more compacted state than the native[25,26]. In our experimental setup we do not observe temporal changes, likely because we cannot capture changes before 30

minutes. However, our data provide a useful look into the next steps in these processes. Other work has shown increased chromatin mobility associated with repair of DSBs minutes to hours after damage[13,14,15,28,29]. Other studies have observed a change in overall coherence of the chromatin after large-scale damage and repair[3,30,31]. Compaction is advantageous early on to signal for certain DDR factors, but, if not reversed, can hinder later stages of repair[26]. Our data reveal that this necessary relaxation occurs over the course of hours following formation of damage foci. Also important to note is that it has recently been shown that chromatin diffusivity is variable when comparing different timescales - i.e. timescales on the order of milliseconds display subdiffusive motion and timescales on the order of seconds display motion closer to Brownian[27]. Our data, taken at timescales on the order of minutes, continues this pattern. Inhibition of proteins in DNA repair pathways (e.g. 53BP1, ATM, SIRT6) have been shown to reduce the increased mobility of chromatin associated with the repair process[13,14,15]. We speculate that the mechanical decoupling works to prevent large scale movements of the damaged domain so that the free ends of the DSBs remain in close proximity, thereby increasing the likelihood that proper rejoining will occur. Additionally, the local decondensation around the damage foci allows access to repair factors. We also observe that one or many of these mechanically independent mechanical regions may be formed within a single nucleus depending on the number of damaged sites in the nucleus.

## Methods

### Cell Culture, Transfection, and Drug Treatments

The human osteosarcoma cell lines, U2OS and U2OS-TRE[5], were cultured in DMEM low glucose media supplemented with 10% FBS and 1% penicillin-streptomycin (Life

Technologies, Grand Island, NY). Cell cycle was not arrested due to possible alterations in gene expression that could bias results. Instead, imaging was continued for an hour after data collection was complete to ensure cells did not undergo mitosis or apoptosis. U2OS-TRE cells were passaged to 35 mm μ-dishes with ibiTreat (ibidi, Verona, WI) and co-transfected with rDNA of GFP-Fib (kind gift from D. Discher, University of Pennsylvania), and either TA-mCherry, TetR-mCherry, TA-KillerRed, or TetR-KillerRed to visualize chromatin dynamics of various sites[5]. U2OS cells were passaged to 35 mm μ-dishes with ibiTreat (ibidi, Verona, WI) and transfected with rDNA of RFP-TRF1, and GFP-Fibrillarin or GFP-53BP1. Cells were transfected using Lipofectamine 3000 transfection reagent (Life Technologies, Grand Island, NY) according to manufacturer's protocol. Cells were washed with PBS and media was changed between 5 and 8 hours post transfection, and experiments were run 24-48 hours post transfection to allow for adequate expression levels. For bleocin DNA damage experiments, cells were treated with 5 ng/mL for 2 hours, at which time cells were washed with PBS and media was changed. For U2OS-TRE cells and consistent with previously established methods[5], photoactivation for all transfection schemes involving TA-mCherry, TA-KillerRed, TetR-mCherry, or TetR-KillerRed was performed using a 15-W SYLVANIA cool white fluorescent bulb for 10 minutes of exposure in a stage UVP (Uvland, CA, USA). This yielded a rate of 15 $J/m^2/s$, which, for 10 minutes of exposure, resulted in 9000 $J/m^2$ being delivered to the dish and a final power of ~9 nJ delivered to the KR ($\sim$1 $\mu m^2$) upon light exposure. Positive and negative controls for imaging with this system in the absence of white-light illumination were previously published[5]. For late-time experiments with TA-KR transfected cells, the culture dish was returned to the incubator for 2 hours after light exposure before imaging.

**Cell Fixation, Immunostaining, and Colocalization Imaging**

Cells in a medium for immunostaining were fixed with methanol-acetone (1:1) for 10 min at −20°C. The fixed cells were dried, then rinsed once with PBS and incubated in blocking buffer (PBS containing the blocking reagent NEN) at 30°C for 30 min. Cells were washed three times with PBST (PBS with Tween 20) buffer and incubated with Alexa Fluor 405 goat anti-mouse immunoglobulin G, Alexa Fluor 488 donkey anti-goat immunoglobulin G conjugate or Alexa Fluor 488 donkey anti-rabbit immunoglobulin G conjugate (Invitrogen). Cell samples were then mounted in drops of PermaFluor (Immunon). Antibodies used in this research were anti-KR (Ab961, Evrogen), anti- H3AcK9 (1:200, Abcam Ab4441), anti- H3DiMeK9 (1:100, Abcam 1220). The Olympus FV1000 confocal microscopy system was employed (Cat. F10PRDMYR-1, Olympus) and FV1000 software was used for acquisition of images. Images were acquired with 488nm and 594 nm, respectively.

**Particle Tracking Imaging and Analysis**

Imaging for particle tracking experiments was done using a 63x, 1.4 NA, oil immersion objective of an inverted microscope (DMI6000, Leica, Buffalo Grove, IL) in a controlled live-cell imaging chamber with humidified 5% CO2 and held at 37°C. Cell nuclei were labeled with 0.5 μg/mL Hoechst 33342 (Life Technologies, Grand Island, NY). Images were taken at multiple (8-12) positions per plate at 3-minute intervals with multiple transfected cells per field of view and multiple particles per cell. Only the bright field, green and/or red channels were acquired with 430-510nm and 515-560nm excitation ranges, respectively, for this time to minimize phototoxicity. Cells did not divide and maintained viability well beyond the duration of the experiment as confirmed by continued imaging for over an hour after the completion of data

collection. Two-dimensional tracking of GFP-Fib, and either TA-mCherry, TetR-mCherry, TA-KillerRed, or TetR-KillerRed as well as RFP-TRF1 and GFP-Fibrillarin or GFP-53BP1 chromatin regions was performed using custom Laptrack71 programs designed in MATLAB (Natick, MA) as previously published[7,32]. Briefly, images were cropped and aligned to remove artifacts including imaging drift, nuclear translation, and nuclear rotation. Therefore, only intranuclear motion of particles was tracked. Particles were then detected through statistical algorithms after calibration of background noise parameters. Particle tracks were then determined by correspondence with succeeding frames. Only persistent tracks of particles present for the full duration of the experiment were used for further analysis. The ensemble-averaged MSD was calculated from the particle tracks as shown in equation (1) where $\tau$ is the lag time.

$$MSD(\tau) = \langle (x_{t+\tau} - x_t)^2 + (y_{t+\tau} - y_t)^2 \rangle \quad (1)$$

Outliers, defined as tracks which were greater than 3 standard deviations away from the ensemble average at the final lag time, were removed from the dataset. The ‘n’ values reported in figure legends represent the number of cells analyzed. For GFP-Fibrillarin, RFP-TRF1, and GFP-53BP1, each cell may have one or multiple tracks, so the total number of particles tracked is greater than n. For TA-mCherry, TetR-mCherry, TA-KillerRed, and TetR-KillerRed, since TA and TetR bind to a specific locus within the chromatin, there is only one track per cell, so the total number of particles tracked exactly equals n. MSD magnitudes were compared at each time point using Student’s t-test. Error bars on MSD plots represent Standard Error of the Mean.

## References


1. Luger K., Dechassa M. L. & Tremethick D. J. New insights into nucleosome and chromatin structure: an ordered state or a disordered affair? *Nat. Rev. Mol. Cell Bio.* **13**, 436-447 (2012).
2. Spagnol S. T. & Dahl K. N. Active cytoskeletal force and chromatin condensation independently modulate intranuclear network fluctuations. *Int. Bio.* **6**, 523-531 (2014).
3. Zidovska A., Weitz D. A. & Mitchison T. J. Micron-scale coherence in interphase chromatin dynamics. *PNAS* **110**, 15555-15560 (2013).
4. Ou H. D. *et al*. ChromEMT: visualizing 3D chromatin structure and compaction in interphase and mitotic cells. *Science* **357**, 1-13 (2017).
5. Lan L. *et al*. Novel method for site-specific induction of oxidative DNA damage reveals differences in recruitment of repair proteins to heterochromatin and euchromatin. *Nuc. Acids Res.*, **42**, 2330-45 (2014).
6. Wei L. *et al*. DNA damage during the G0/G1 phase triggers RNA-templated, Cockayne syndrome B-dependent homologous recombination. *PNAS*, E3495-E3504 (2015).
7. Booth-Gauthier E. A., Alcoster T. A., Yang G. & Dahl K. N. Force-induced changes in subnuclear movement and rheology. *Biophys. J.* **103**, 2423-2431 (2012).
8. Kleiner R. E., Verma P., Molloy K. R., Chait B.T. & Kapoor T. M. Chemical proteomics reveals a γH2AX-53BP1 interaction in the DNA damage response. *Nat. Chem. Biol.* **11**, 807-814 (2015).
9. Lu D. *et al*. Nuclear GIT2 is an ATM substrate and promotes DNA repair. *Mol. Cell. Bio.* **35**, 1081-1096 (2015).
10. Rademakers S. *et al*. Xeroderma pigmentosum group A protein loads as a separate factor onto DNA lesions. *Mol. Cell Biol.* **23**, 5755-5767 (2003).
11. Kruhlak M. J. *et al*. Changes in chromatin structure and mobility in living cells at sites of DNA double-strand breaks. *J. Cell Biol.* **172**, 823-834 (2006).
12. Strickfaden H. *et al*. Poly(ADP-ribosyl)ation-dependent transient chromatin decondensation and histone displacement following laser microirradiation. *J. Biol. Chem.* **291**, 1789-1802 (2016).
13. Dimitrova N., Chen Y. M., Spector D. L. & de Lange T. 53BP1 promotes NHEJ of telomeres by increasing chromatin mobility. *Nature* **456**, 524-528 (2008).
14. Becker A., Durante M., Taucher-Scholz G., & Jakob B. ATM Alters the Otherwise Robust Chromatin Mobility at Sites of DNA Double-Strand Breaks (DSBs) in Human Cells. *PLOS One* **9**, 1-10 (2014).
15. Gao Y. *et al.* SIRT6 facilitates directional telomere movement upon oxidative damage. *Scientific Reports* **8**, 1-12 (2018).
16. Aymard F. *et al.* Transcriptionally active chromatin recruits homologous recombination at DNA double strand breaks. *Nat Struct Mol Biol* **21**, 366-374 (2014).
17. Clouaire T., & Legube G. DNA double strand break repair pathway choice: a chromatin based decision? *Nucleus* **6**, 107-113 (2015).
18. Booth E. A., Vane E. W., Dovala D. & Thorner J. A Forster Resonance Energy Transfer (FRET)-based System Provides Insight into the Ordered Assembly of Yeast Septin Hetero-octamers. *J. of Biol. Chem.* **290**, 28388-28401 (2015).

19. Jakob B. *et al*. DNA double-strand breaks in heterochromatin elicit fast repair protein recruitment, histone H2AX phosphorylation and relocation to euchromatin. *Nuc. Acids Res.* **39**, 6489-6499 (2011).
20. Schultz L. B., Chehab N. H., Malikzay A. & Halazonetis T. D. p53 Binding Protein 1 (53BP1) Is an Early Participant in the Cellular Response to DNA Double-Strand Breaks. *J. Cell Bio.* **151**, 1381-1390 (2000).
21. Rappold I., Iwabuchi K., Date T. & Chen J. Tumor Suppressor p53 Binding Protein 1 (53BP1) Is Involved in DNA Damage–signaling Pathways. *J. Cell Bio.* **153**, 613-620 (2001).
22. Chiolo I., Tang J., Georgescu W. & Costes S. V. Nuclear dynamics of radiation-induced foci in euchromatin and heterochromatin. *Mutat Res.* **750**, 1-22 (2014).
23. Caridi C. P. *et al.* Nuclear F-actin and myosins drive relocalization of heterochromatic breaks. *Nature.* **559**, 54-60 (2018).
24. Spagnol S. T., Armiger T. J. & Dahl K. N. Mechanobiology of Chromatin and the Nuclear Interior. *Cell Mol Bioeng.* **9**, 268-276 (2016).
25. Khurana S. *et al.* A Macrohistone Variant Links Dynamic Chromatin Compaction to BRCA1-Dependent Genome Maintenance. *Cell Rep.* **8**, 1049-1062 (2014).
26. Burgess R. C., Burman B., Kruhlak M. J. & Misteli T. Activation of DNA Damage Response Signaling by Condensed Chromatin. *Cell Rep.* **9**, 1703-1717 (2014).
27. Mine-Hattab J., Recamier V., Izeddin I., Rothstein R. & Darzacq X. Multi-scale tracking reveals scale-dependent chromatin dynamics after DNA damage. *MBoC* **28**, 3323-3332 (2017).
28. Krawczyk P. M., Borovski T., Stap J., Cijsouw T., ten Cate R., Medema J. P., Kanaar R., Franken N. A. P., & Aten J. A. Chromatin mobility is increased at sites of DNA double-strand breaks. *J of Cell Sci* **125**, 2127-2133 (2012).
29. Jakob B., Splinter J., Durante M., & Taucher-Scholz G. Live cell microscopy analysis of radiation-induced DNA double-strand break motion. *PNAS* **106**, 3172-3177 (2009).
30. Mine-Hattab J., & Rothstein R. DNA in motion during double-strand break repair. *Trends Cell Biol.* **23**, 1-17 (2013).
31. Girst S., Hable V., Drexler G. A., Greubel C., Siebenwirth C., Haum M., Friedl A. A., & Dollinger G. Subdiffusion Supports Joining Of Correct Ends During Repair Of DNA Double-Strand Breaks. *Scientific Reports* **3**, 1-6 (2013).
32. Yang G., Matov A. & Danuser G. Reliable tracking of large scale dense antiparallel particle motion for fluorescence live cell imaging. Proceedings of Computer Society Conference on Computer Vision and Pattern Recognition IEEE; July 2005; p. 1-9.

# Chapter IV

## Global DNA Damage and Repair in Breast Cancer Cells

### Introduction

In addition to the medical importance, breast cancer has become a model for patient-specific diversity. Triple negative breast cancers, with dysregulated estrogen receptors, progesterone receptors, and the HER2 gene represent 15-20% of all breast cancers are the most difficult to treat. Of these breast cancers and others, cell lines with varying, well-studied properties have been developed to better understand patient-specific diversity including resistance to chemotherapeutic drugs. Platinum-based drugs including cisplatin work well for treatment of triple negative breast cancers, especially during the first round of treatment. However, drug resistance develops in most patients in a year after the first round of treatment. Of the patients that experience relapse, only 1 in 5 survive beyond 5 years.[1]

Cisplatin binds the N7 in guanines in close proximity, either along the chain forming intrastrand dimers or across the double strand forming interstrand crosslinks.[1] Cells, including cancer cells, remove DNA breaks through endogenous mechanisms, but most cells lack the ability to remove large-scale crosslinking. After crosslinking and crosslinked lesions, DNA double strand breaks emerge from replication fork damage ultimately leading to cellular apoptosis.[2,3] Unfortunately, for screening purposes related to treatment options, quantifications of initial DNA-cisplatin lesions do not appear to predict the outcome of cisplatin related treatments on ultimate cell death.[2]

Cisplatin resistance mechanisms are organized into three areas: (i) control of the intracellular concentration of cisplatin, including uptake or outward efflux movement of

cisplatin; (ii) modification and inactivation of cisplatin using the cell's detoxification machinery; and (iii) DNA repair mechanisms after damage including Nucleotide Excision Repair (NER) or Non-Homologous End Joining (NHEJ). NER is used to remove cisplatin adducts and crosslinks, while NHEJ is used to repair DNA damage resulting from a replication fork encountering a Cisplatin adduct or crosslink. Resistance and sensitivity to Cisplatin seem be governed by the same DNA damage repair pathways, as increased NER activity usually indicates resistance while reduced NER activity usually indicates sensitivity.[1,4] NER is the main mechanism of Cisplatin induced damage repair.[5] Olive and Banath 2009 showed that early (6hr) formation of γH2AX foci did not predict ultimate cell death in human cervical carcinoma (SiHa), human colon carcinoma (WiDr), and hamster parental (V79-4) cells, but that persistent (24hr) γH2AX foci were a good indication that Cisplatin treatment would ultimately lead to cell death.[3]

We have developed methods for measuring changes to chromatin structure, mobility and stiffness in the nuclei of cells.[6] Chromatin mobility during DNA damage repair shows increased chromatin mobility at damage sites[7] and loss of coherence between disparate nuclear regions.[8] Physiologically induced DNA damage has recently been shown to be repaired in a similar way - during sleep chromatin mobility in neurons is increased, while DNA damage load is decreased.[9]

Previous work has shown that the triple negative breast cancer cell line MDA-MB-231 is sensitive to Cisplatin treatment.[10] In the same study, two other triple negative breast cancer cell lines, HCC1806 and Hs578T, were shown to have neutral IC50 values indicating that they are neither particularly resistant nor sensitive to treatment with Cisplatin. The reason for their particular difference in sensitivity is not clear, but as the primary therapeutic mechanism of Cisplatin is to cause DNA damage, the most likely difference is probably an attenuated DNA damage response in MDA-MB-231 cells.

## Results

### Baseline nuclear rheology of 3 breast cancer cell types

Here, we examine the chromatin motility in three triple negative breast cancer cell lines and healthy primary cells. The control cells are primary human mammary epithelial cells (hMECs). HCC1806 are a non-metastatic primary tumor cell line that is mostly insensitive to Cisplatin. Hs578T is a metastatic cell line, also not sensitive to Cisplatin. MDA-MB-231 is a metastatic, pleural effusion cell line that has been shown to be sensitive to Cisplatin.[10]

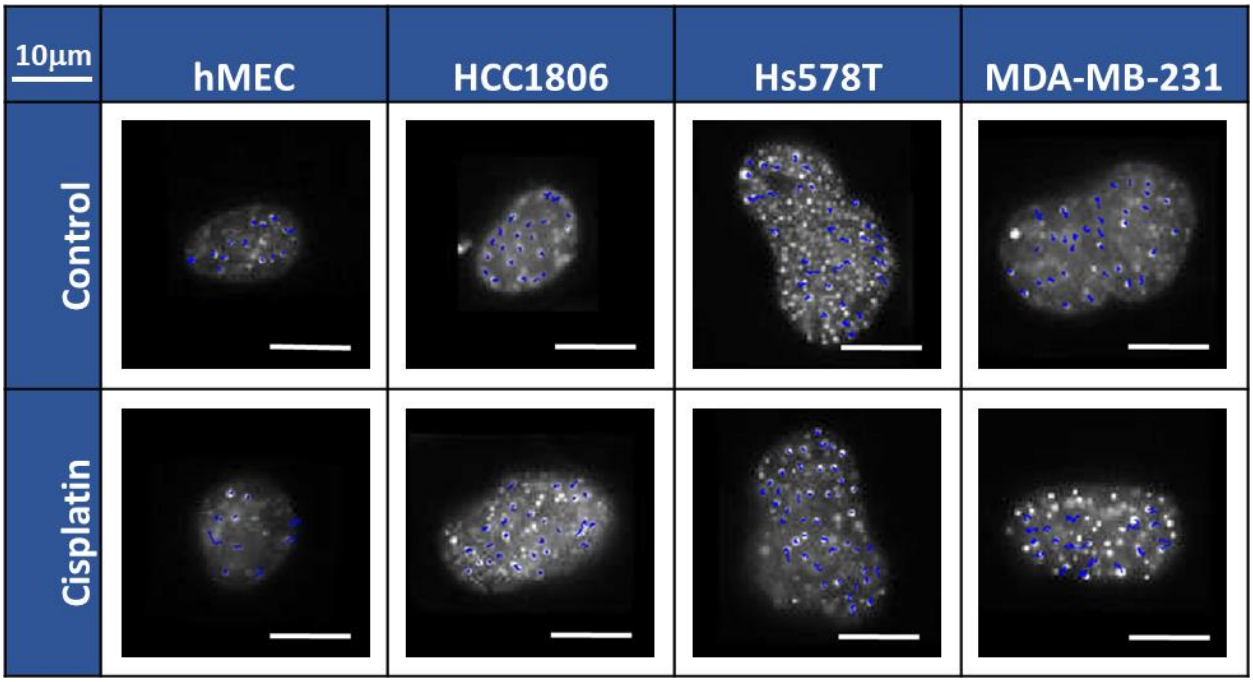


***Figure 4.1: Nuclei transfected with GFP-UBF1 superimposed with trajectories of particle motions.*** *Representative images of nuclei in live cells from each cell type with and without treatment. Images were processed in MATLAB to subtract translational and rotational motion of nuclei so that only the motion of individual particles was tracked, not motion of the nuclei themselves. Blue lines show the centroids of particle trajectories mapped by algorithm for images taken every 3 min for 1 hr. In some cases, spots do not have accompanying arrows*

*suggesting that points do not persist throughout the sampling time. Culture conditions are Untreated (Control) and treated with 200 μM Cisplatin for 2 hrs (Cisplatin). Error bars are 10 μm.*

To establish chromatin mobility, we utilized Sensors from IntraNuclear Kinetics (SINK), which is a particle tracking technique developed in our lab.[6,7,11,12,13,14] Briefly, cells were transfected with GFP-UBF1, a chromatin-binding protein, and images of live cells were taken every 3 min for 1 hr. Images of nuclei were aligned in MATLAB to remove any translational or rotational motion of the nucleus associated with cell movements or nuclear movements within the cell. Thus, only chromatin fluctuations within the nucleus are measured (Figure 4.1). Mean Squared Displacements (MSDs) were calculated from tracked GFP-UBF1 foci, and plotted versus lag time, τ, on log-log coordinates (Figure 4.2). From the log-log MSD versus τ, baseline chromatin motion of Control, HCC1806, and MDA-MB-231 chromatin is similar whereas the motion of Hs578T chromatin is statistically higher at longer lag times.

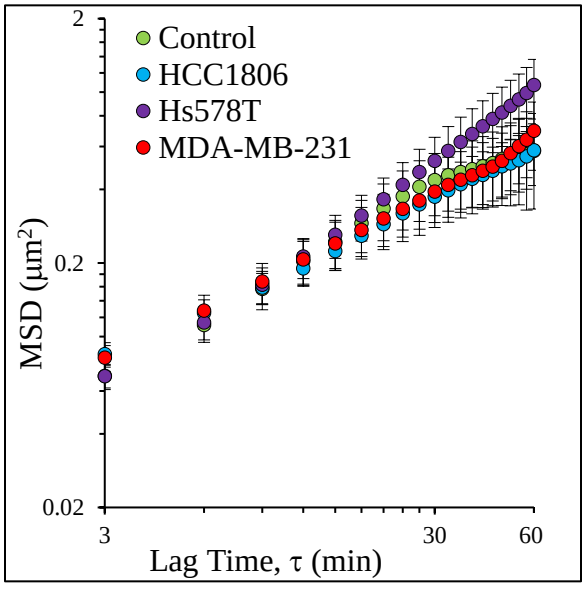


***Figure 4.2: Chromatin mobility in control cells and cancer cell lines from particle tracking.*** *SINK particle tracking data of GFP-UBF1 foci in untreated Control cells (green, n=12 cells, N=95 tracks), HCC1806 cells (blue, n=65 cells, N=367 tracks), Hs578T cells (purple, n=64 cells, N=1911 tracks), and MDA-MB-231 cells (red, n=64 cells, N=420 tracks). Error bars are SEM.*

*Untreated cells show surprisingly similar chromatin mobility aside from Hs578T cells. Confirmed by 95% confidence interval t-test.*

**Chromatin treatment of control cells shows stiffening with Cisplatin**

To determine the baseline mechanical response of chromatin to Cisplatin treatment in healthy cells, hMECs were treated with 200 μM Cisplatin for 2 hrs immediately preceding particle tracking. Measuring chromatin mobility by tracking GFP-UBF1 foci revealed that the chromatin in control cells becomes less mobile in response to Cisplatin treatment (Figure 4.3). Reduced mobility (higher MSD versus τ) is an increased stiffening of the chromatin. Since the media is changed between drug treatment and imaging, this data shows the early (2-3 hr) rheological and biological response of the chromatin to Cisplatin induced damage, not the damage event itself. This data is consistent with previous studies of DNA damage that showed stiffening of chromatin in response to DNA the repair process.[7,9]

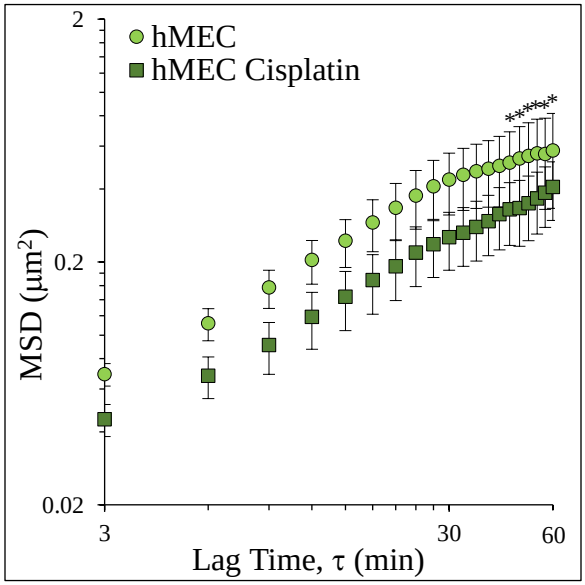


***Figure 4.3: Stiffening of chromatin in control cells with Cisplatin treatment.*** *MSD of GFP-UBF1 foci in untreated Control cells (light green, n=12 cells, N=95 tracks) and Cisplatin treated control cells (dark green, n=12 cells, N=83 tracks) versus τ. Error bars are SEM. 95% confidence interval t-test confirms that MSD are statistically distinct except for last six lag times, which are marked with an *. Due to the method of calculating MSD, these values have greater variance than MSD values for lower lag times.*

**Breast cancer cell lines insensitive to Cisplatin are similar to control cells**

To determine how chromatin mobility in Cisplain-insensitive breast cancer cell lines responds to Cisplatin treatment, HCC1806 and Hs578T cells were treated with 200 μM Cisplatin for 2 hr immediately preceding particle tracking. Tracking GFP-UBF1 foci to measure the mobility of the chromatin in these cells after Cisplatin treatment revealed a similar decrease in the mobility of the chromatin in both cell lines to that in Control cells (Figure 4.4). This indicates that that healthy cells and non-sensitive cancer cells respond similarly to DNA damage induced by Cisplatin. As noted previously, the baseline chromatin mobility in Hs578T cells was slightly higher than the other cell types analyzed. This trend is echoed after Cisplatin treatment as the decrease in mobility of Hs578T chromatin is less pronounced than the decrease in chromatin mobility in control and HCC1806 cells.

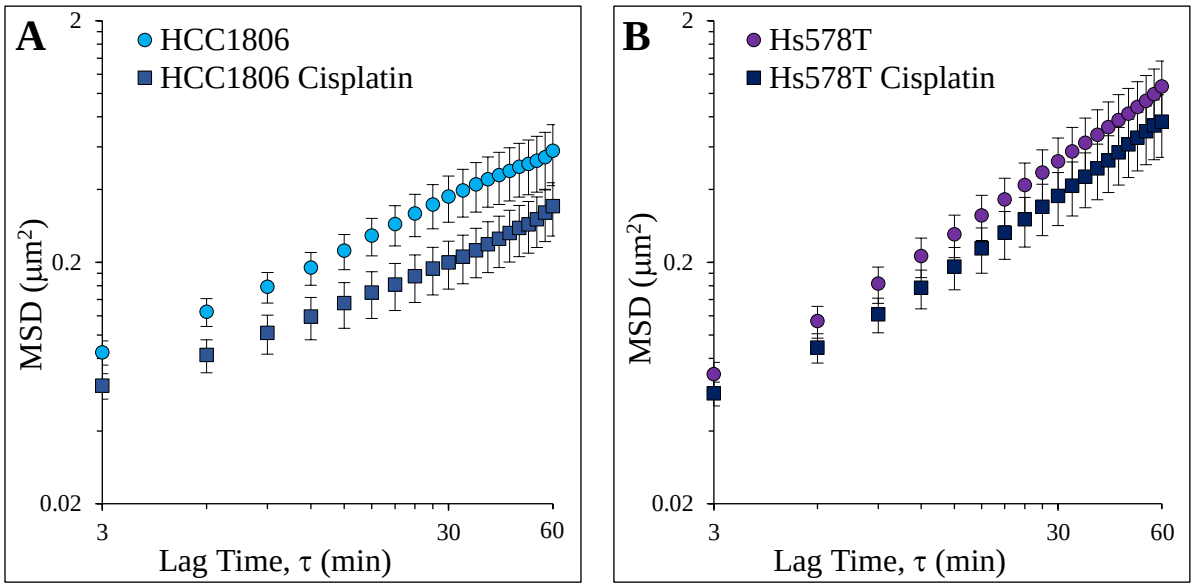


***Figure 4.4: Mobility of chromatin is reduced after Cisplatin treatment in cisplatin-insensitive breast cancer cell lines. A)*** *MSD of GFP-UBF1 foci in untreated (light blue, n=65 cells, N=367 tracks) and Cisplatin treated HCC1806 cells (dark blue, n=60 cells, N=468 tracks) versus* $\tau$ *shows reduced chromatin motility with Cisplatin treatment. MSD values for all lag times are statistically different as confirmed by 95% confidence interval t-test.* ***B)*** *MSD of GFP-UBF1 foci*

*in untreated (light purple, n=64, N=1911 tracks) and Cisplatin treated Hs578T cells (dark purple, n=56 cells, N=1168 tracks) versus τ similarly show reduced mobility. Error bars are SEM. MSD values for all lag times are statistically different as confirmed by 95% confidence interval t-test.*

**Cisplatin-sensitive breast cancer cell line shows altered response to Cisplatin**

MDA-MB-231 cells, sensitive to Cisplatin[10], were treated with 200 μM Cisplatin for 2 hr. Unlike control and non-sensitive breast cancer cell lines, no significant change in chromatin mobility could be detected after treatment with Cisplatin (Figure 4.5). This may indicate that cell survival after Cisplatin treatment is in some way related to a change in the rheological properties of the chromatin network.

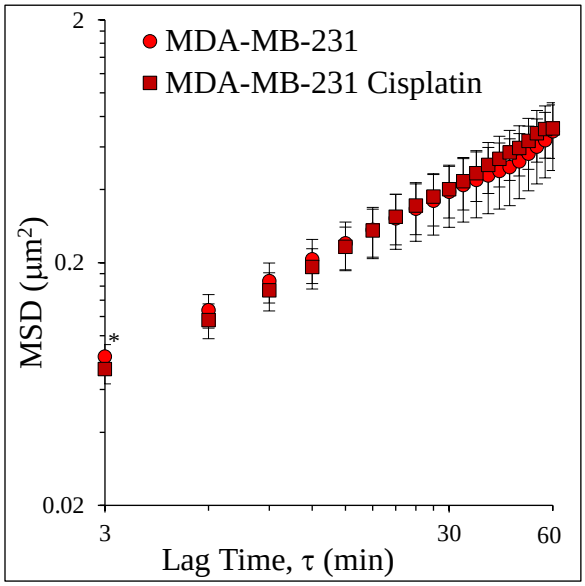


***Figure 4.5: Mobility of chromatin is unchanged after Cisplatin treatment in cisplatin-sensitive breast cancer cell line.*** *MSD of MDA-MB-231 cells (light red, n=64 cells, N=420 tracks) and Cisplatin-treated MDA-MB-231 cells (dark red, n=34 cells, N=176 tracks) versus τ shows no significant difference. Error bars rare SEM. MSD values for all lag times except the first, marked by an *, are statistically different as confirmed by 95% confidence interval t-test.*

**Cisplatin-sensitive breast cancer cell line shows dose dependent formation of damage foci marked by γH2AX.**

To ensure that the lack of change in MDA-MB-231 cells was due to a lack of mechanical response to damage rather than a lack of damage itself, hMEC and MDA-MB-231 cells were treated with 200μM cisplatin as in particle tracking experiments, then fixed and stained with Hoechst 33342 as well as immunostained for γH2AX. MDA-MB-231 cells had significantly increased γH2AX signal from hMECs indicating that not only was damage present in MDA-MB-231 cells, but that there was significantly more damage than in Control cells. To investigate the dose dependence of cisplatin induced DNA damage in cisplatin-sensitive cells, MDA-MB-231 cells were treated with 2mM (10 times the dose of cisplatin used in particle tracking experiments), then fixed and stained with Hoechst and immunostained for γH2AX. Significantly more damage foci were detected in MDA-MB-231 cells treated with 10 times the particle tracking dose as those treated with exactly the particle tracking dose. This indicates, unsurprisingly, that formation of damage foci in response to cisplatin treatment is dose dependent. In ImageJ, masks were made for each nucleus using the Hoechst channel. Damage foci were then counted for each nucleus using a standard set of settings and parameters in the Analyze Particles function in ImageJ. Cells were grouped based on the number of γH2AX foci per nucleus into 0-19, 20-39, and 40+ groups. The bar graphs in Figure 4.6A show the proportion of each of these groups under each experimental condition. Figures 4.6B-D show representative images of γH2AX stained hMECs with the particle tracking cisplatin dose, MDA-MB-231 cells with the particle tracking cisplatin dose, and MDA-MB-231 cells with ten times the particle tracking cisplatin dose, respectively.

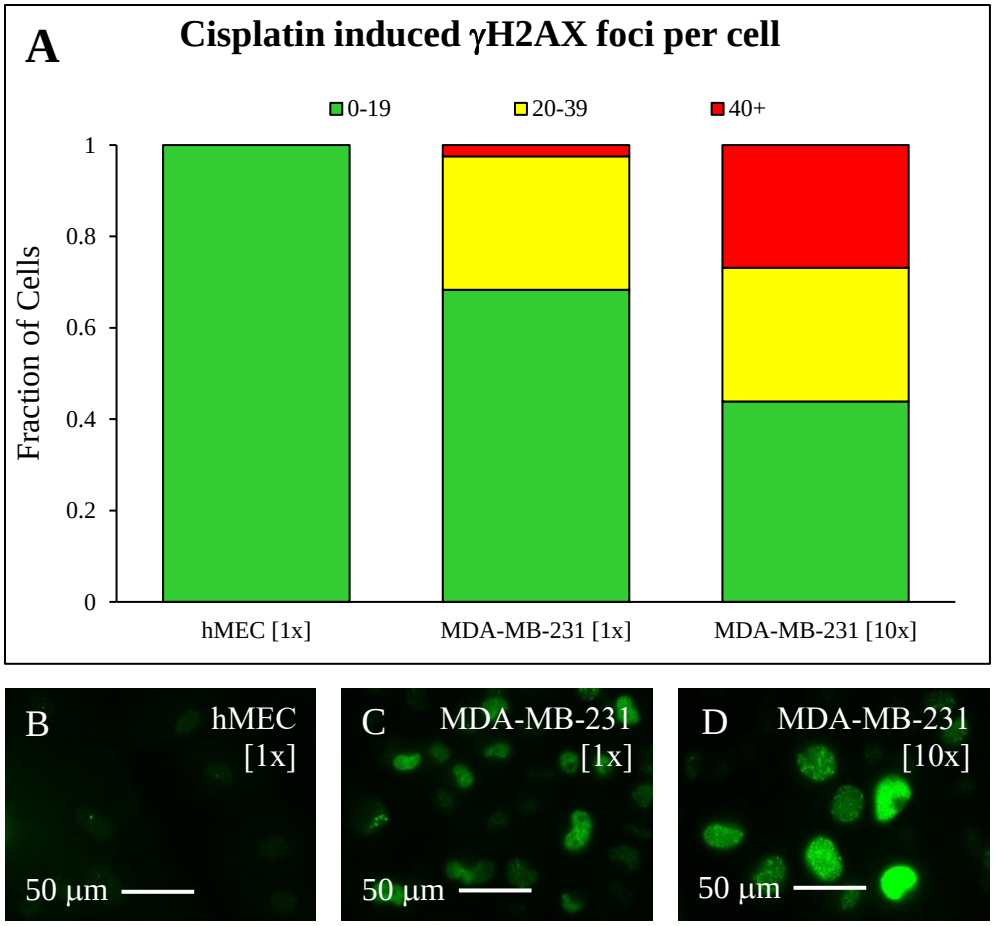


***Figure 4.6: Damage foci in MDA-MB-231 cells increase dose-dependently with Cisplatin treatment. A)*** *Bar graph showing fraction of cells in each condition with between 0 and 19 γH2AX foci (green), 20 and 39 γH2AX foci (yellow), and greater than or equal to 40 γH2AX foci (red).* ***B)*** *Representative image of hMEC cells treated with 200μM cisplatin and immunostained for γH2AX. Scale bar is 50μm.* ***C)*** *Representative image of MDA-MB-231 cells treated with 200μM cisplatin and immunostained for γH2AX. Scale bar is 50μm.* ***D)*** *Representative image of MDA-MB-231 cells treated with 2mM cisplatin and immunostained for γH2AX. Scale bar is 50μm.*

**$D_{eff}$ calculated with β held constant within cell lines**

To gain more insight into the particular biophysical components that contribute to the trends observed by comparing chromatin mobility, the MSDs of all experiments were fit to the power law model: $MSD(\tau) = D_{eff} * \tau^{\beta}$ where τ is Lag Time, $D_{eff}$ is related to chromatin condensation,

and β is related to force propagation.[6] Untreated and Cisplatin treated cells of the same cell type had similar β values to each other, but different β values between different cell types. $D_{eff}$ values in cisplatin treated cells were all significantly lower than their respective untreated counterparts in Control, HCC1806, and Hs578T cells, but $D_{eff}$ values were similar in MDA-MB-231 cells. This indicates that the difference observed in chromatin mobility change between MDA-MB-231 cells and the other three cell types are more related to chromatin condensation than to force propagation throughout the nucleus. Since the β values within each cell type were similar, these β values were standardized for each cell type and $D_{eff}$ values were recalculated using the standardized β values. Figure 4.7A shows the adjusted $D_{eff}$ values calculated from the MSDs of the particle tracking experiments and the standardized β values for each cell type. The adjusted $D_{eff}$ values of untreated and cisplatin treated MDA-MB-231 cells are statistically similar to each other while the untreated and cisplatin treated adjusted $D_{eff}$ values for the other three cell types are all significantly different from each other. Figure 4.7B is a cartoon illustrating our proposed explanation of the difference between MDA-MB-231 and the other cell lines tested.

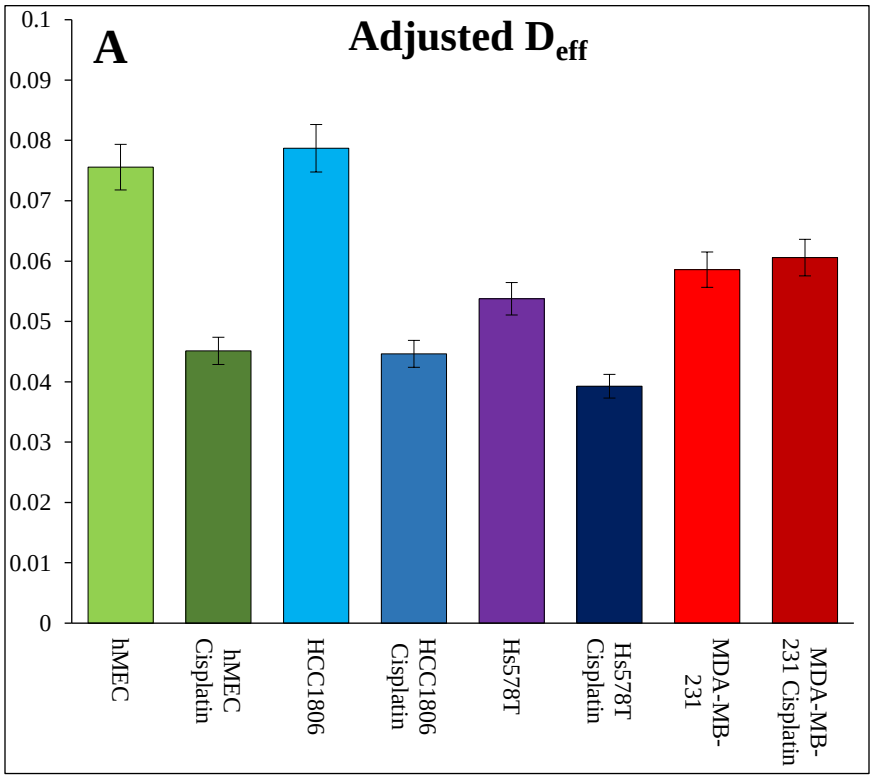

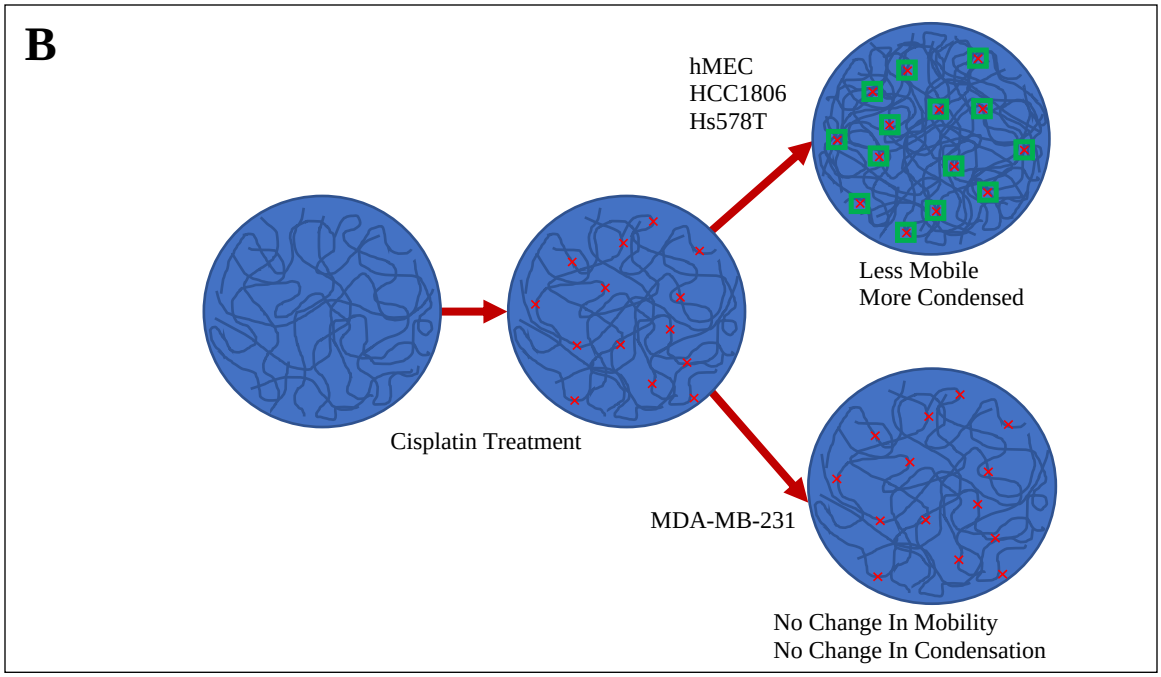


***Figure 4.7: Chromatin condensation state and proposed model of damage response. A)*** *Adjusted $D_{eff}$ values calculated from standardized $\beta$ values. Error bars are 95% confidence interval.* ***B)*** *Cartoon of our proposed mechanism of MDA-MB-231 senstivity.*

## Discussion

Measuring baseline chromatin mobility in hMEC, HCC1806, Hs578T, and MDA-MB-231 cells using SINK revealed that at early lag times all of these cells types had similar chromatin mobility. At later lag times, H2578T, had somewhat greater chromatin mobility than the others, but some amount of variability in the physical properties of different cell types is to be expected. MDA-MB-231 and Hs578T were chosen to compare two metastatic cell lines with differing Cisplatin sensitivities, HCC1806 to compare a non-metastatic breast cancer response, and hMECs so that to compare the response of the surrounding healthy tissue.

Non-disease hMEC cells had reduced chromatin mobility after treatment with cisplatin, suggesting that the normal DNA damage response to cisplatin-induced DNA damage is to limit

mobility of the chromatin network. This seems to be in contrast with previous findings where chromatin mobility was increased in response to DNA damage.[7] One possible explanation for this discrepancy is that previous studies focused upon the sites of DNA damage, while this study focuses on the chromatin network as a whole. At individual damage sites mobility may very well be increased. Increased mobility at damage sites may "take up the slack" from the rest of the network reducing the mobility of other regions of chromatin. This study found no direct evidence of this, so more investigation is needed. Another explanation of this discrepancy could be differences in repair pathways. Previous studies focused upon double strand break repair pathways such as Homologous Recombination and Non-Homologous End Joining, the most likely repair pathway being measured by this study is Nucleotide Excision Repair.

When the two cell lines shown by Uhr et al. to be neutral to cisplatin (HCC1806 and Hs578T) were analyzed with SINK they displayed a similar reduction in chromatin mobility to healthy Control cells in response to cisplatin treatment. As it is unlikely that the pathways controlling intracellular concentration of cisplatin and detoxification of cisplatin are affecting chromatin mobility, it is reasonable to assume that the similar response of chromatin mobility is due to similar activity of the DNA damage response regarding cisplatin-induced damage. One possible explanation of this relationship is that Cisplatin-sensitive cells are unable to stiffen their chromatin in response to Cisplatin-induced DNA damage which is necessary for repair to proceed. As chromatin stiffened in hMEC, HCC1806, and Hs578T cells, an alteration in machinery related to the third mechanism seems to be responsible for the lack of change in the mobility of chromatin in cisplatin-sensitive cells. Both sensitivity to cisplatin and the absence of a mobility change after cisplatin treatment indicate that MDA-MB-231 cells are deficient in the repair machinery necessary to remove and mend cisplatin crosslinks and adducts.

However, when the cell line shown by Uhr et al. to be sensitive to cisplatin (MDA-MB-231) was analyzed with SINK, no change in chromatin mobility could be detected after treatment with cisplatin indicating an inability to repair cisplatin-induced damage. As SINK measures neither the intracellular concentration of cisplatin or the cells' ability to detoxify cisplatin, it remains unknown whether or not these mechanisms of cisplatin resistance are inhibited in any way to amplify the sensitivity of MDA-MB-231 cells to cisplatin, but it is reasonable to assume that these mechanisms are not, to a significant degree at least, working against the sensitivity to cisplatin produced by MDA-MB-231 cells' lack of repair capability.

Cisplatin may trigger the DNA damage response in a few ways: either adducts will trigger an NER response, or crosslinks will generate damage after failed transit of polymerases or helicases which usually cause single or double strand breaks. It is generally accepted that the latter form of damage only occurs as cells transit S phase, and as cells are only exposed to cisplatin for 2 hours before analysis with SINK, the former is the most likely source of DNA damage.

Previous studies have shown that early accumulation of damage foci is not predictive of cisplatin treatment efficacy, but long term persistence is.[2,3] However, SINK is able to detect changes, or lack thereof, in the chromatin mobility of cells treated with cisplatin that are predictive of sensitivity to cisplatin treatment.

A Cisplatin sensitive cell line unable to relax chromatin in response to cisplatin DNA damage is consistent with findings of Zada et al. 2019 showing that sleep deprivation inhibits chromatin relaxation and promotes accumulation of double strand breaks.[9]

## Methods

### Cell Culture

HCC1806 cells were cultured in DMEM high glucose media supplemented with 10% FBS and 1% penicillin-streptomycin (Life Technologies, Grand Island, NY). Hs578T cells were cultured in RPMI 1640 media supplemented with 10% FBS and 1% penicillin-streptomycin (Life Technologies, Grand Island, NY). MDA-MB-231 cells were cultured in DMEM high glucose media supplemented with 10% FBS and 1% penicillin-streptomycin (Life Technologies, Grand Island, NY). Primary hMECs were cultured in Complete Growth Medium from ATCC. Unlike the other cell types, hMECs were trypsinized during passaging with Trypsin-EDTA for Primary Cells (ATCC, Manassas, VA) and neutralized with Trypsin Neutralizing Solution (ATCC, Manassas, VA). The other cell types were all trypsinized with 0.25% Trypsin-EDTA with phenol red (Thermo Scientific, Waltham, MA) and neutralized with their respective FBS-containing culture media.

Cell cycle was not arrested due to possible alterations in gene expression that could bias results. Instead, imaging was continued for an hour after data collection was complete to ensure cells did not undergo mitosis or apoptosis.

### Transfection

All cell types were passaged to 35 mm ibiTreat μ-dishes (ibidi, Fitchburg, WI) and co-transfected with rDNA of GFP-UBF1 (kind gift from D. Discher, University of Pennsylvania). Cells were transfected using Lipofectamine 3000 transfection reagent (Life Technologies, Grand Island, NY) according to manufacturer's protocol. Cells were washed with PBS and media was

changed between 5 and 8 hours post transfection, and experiments were run 24–48 hours post transfection to allow for adequate expression levels.

**Drug Treatments**

For cisplatin DNA damage experiments, cells were treated with 200μM for 2 hours. Cells were washed with PBS and media was changed immediately before and at the conclusion of drug treatments. In dose-dependent investigation of cisplatin-induced DNA damage "1x Cisplatin Dose" indicates 200μM cisplatin treatment, and "10x Cisplatin Dose" indicates 2mM cisplatin treatment.

**Particle Tracking**

Imaging for particle tracking experiments was done using a 63x, 1.4 NA, oil immersion objective of an inverted microscope (DMI6000, Leica, Buffalo Grove, IL) in a controlled live-cell imaging chamber with humidified 5% $CO_2$ and held at 37 °C. Cell nuclei were labeled with 0.5 μg/mL Hoechst 33342 (Life Technologies, Grand Island, NY). Images were taken at multiple (8–12) positions per plate at 3-minute intervals with multiple transfected cells per field of view and multiple particles per cell. Only the bright field and green channels were acquired with 430–510 nm excitation ranges for this time to minimize phototoxicity. Cells did not divide and maintained viability well beyond the duration of the experiment as confirmed by continued imaging for over an hour after the completion of data collection. Two-dimensional tracking of GFP-UBF1 chromatin regions was performed using custom Laptrack71 programs designed in MATLAB (Natick, MA) as previously published.[11] Briefly, images were cropped and aligned to remove artifacts including imaging drift, nuclear translation, and nuclear rotation. Therefore,

only intranuclear motion of particles was tracked. Particles were then detected through statistical algorithms after calibration of background noise parameters. Particle tracks were then determined by correspondence with succeeding frames. Only persistent tracks of particles present for the full duration of the experiment were used for further analysis. The ensemble-averaged MSD was calculated from the particle tracks as shown in the equation $MSD(\tau) = \langle (x_{\tau+3} - x_\tau)^2 + (y_{\tau+3} - y_\tau)^2 \rangle$, where $\tau$ is the lag time.

Outliers, defined as tracks which were greater than 3 standard deviations away from the ensemble average at the final lag time, were removed from the dataset. The 'n' values reported in figure legends represent the number of cells analyzed. Almost all nuclei contained more than one track and many cells had greater than a dozen, so the total number of particles tracked is significantly greater than n. MSD magnitudes were compared at each time point using Student's t-test. Error bars on MSD plots represent Standard Error of the Mean.

Statistical algorithms were used to both calibrate for background noise and identify and track persistent GFP-UBF1 foci. Mean Squared Displacements (MSDs) were calculated from these tracks, while outliers, defined by being 3 standard deviations away from the mean, were removed.

**Immunostaining**

Cells grown, transfected, and, if applicable, treated with cisplatin in 35mm ibiTreat m-dishes (ibidi, Fitchburg, WI) were fixed with 3.7% formaldehyde for 15 minutes, then rinsed 3 times with 1X PBS. Cells were permeabilized with 0.2% Triton X-100 for 15 minutes, then rinsed 3 times with 1X PBS. Cells were blocked against non-specific binding with 0.2% BSA for 1 hour, then rinsed 3 times with 1X PBS. Primary antibody staining was accomplished with

mouse anti-human/mouse γH2AX (Thermo Scientific, Waltham, MA) diluted in 0.2% BSA for 1 hour while being protected from light, then rinsed 3 times with 1X PBS. Secondary antibody staining was accomplished with Alexa Fluor 488 goat anti-mouse antibodies (Life Technologies, Grand Island, NY). Simultaneously, the secondary antibodies and Hoechst 33342 (Life Technologies, Grand Island, NY) were diluted in 0.2% BSA and used to label cells for 1 hour while being protected from light, then rinsed 3 times with 1X PBS. The third rinse with 1X PBS was left in the 35mm ibiTreat m-dish for storage and imaging.

## References


1. Cheun Y., Koag M., Naguib Y. W., Ouzon-Shubeita H., Cui Z., Pakotiprapha D., & Lee S. Synthesis, structure, and biological evaluation of a platinum-carbazole conjugate. *Chem Biol Drug Des*. **91**, 116-125 (2017).
2. Brozovic A. et al. Cisplatin sensitivity is related to late DNA damage processing and checkpoint control rather than to the early DNA damage response. *Mutation Research*. **670**, 32-41 (2009).
3. Olive P. & Banath J. P. Kinetics of H2AX Phosphorylation After Exposure to Cisplatin. *Clinical Cytometry*. **76B**, 79-90 (2009).
4. Ferry K. V., Hamilton T. C., & Johnson S. W. Increased Nucleotide Excision Repair in Cisplatin-Resistant Ovarian Cancer Cells: Role of ERCC1-XPF. *Biochemical Pharmacology*. **60**, 1305-1313 (2000).
5. Rabik C. A. & Dolan M. E. Molecular Mechanisms of Resistance and Toxicity Associated with Platinating Agents. *Cancer Treatment Review*. **33**, 1-26 (2007).
6. Spagnol S. T. & Dahl K. N. Active cytoskeletal force and chromatin condensation independently modulate intranuclear network fluctuations. *Int. Bio.* **6**, 523-531 (2014).
7. Whitefield D. B., Spagnol S. T., Armiger T. J., Lan L., & Dahl K. N. Quantifying site-specific chromatin mechanics and DNA damage response. *Scientific Reports*. **8**, 1-9 (2018).
8. Zidovska A., Weitz D. A. & Mitchison T. J. Micron-scale coherence in interphase chromatin dynamics. *PNAS* **110**, 15555-15560 (2013).
9. Zada D., Bronshtein I., Lerer-Goldshtein T., Garini Y., & Appelbaum L. Sleep increases chromosome dynamics to enable reduction of accumulating DNA damage in single neurons. *Nature Communications*. **10**, 1-12 (2019).
10. Uhr et al. Understanding drugs in breast cancer through drug sensitivity screening. *SpringerPlus*. **4**, 1-11 (2015).
11. Booth-Gauthier E. A., Alcoster T. A., Yang G. & Dahl K. N. Force-induced changes in subnuclear movement and rheology. *Biophys. J.* **103**, 2423-2431 (2012).

12. Booth E. A., Spagnol S. T., Alcoster T. A., & Dahl K. N. Nuclear stiffening and chromatin softening with progerin expression leads to an attenuated nuclear response to force. *Soft Matter*. 1-7 (2015).
13. Armiger T. J., Spagnol S. T., & Dahl K. N. Nuclear mechanical resilience but not stiffness is modulated by αII-spectrin. *Journal of Biomechanics*. **8**, 49-55 (2016).
14. Armiger T. J., Lampi M. C., Reinhart-King C. A., & Dahl K. N. Determining mechanical features of modulated epithelial monolayers using subnuclear particle tracking. *Journal of Cell Science*. **131**, 1-6 (2018).

# Chapter V

## Chromatin Margination During HSV-1 Infection

### Introduction

With nearly every single person that reaches adulthood being seropositive for at least one member of the Herpesviridae family, these viruses are among the most ubiquitous minor human pathogens in existence and are the causative agent of many (usually) non-life-threatening diseases from cold sores to genital herpes and chicken pox to mono.[1] All herpesviruses are double-stranded DNA viruses that are released by budding and are therefore also all enveloped viruses.[2] Herpesviruses are able to establish two types of infections – lytic, during which the viruses replicate, and latent, during which the viral genome may lay dormant for years – both are established within the nucleus of their host cell.[3,4] Herpesviruses are divided into three subfamilies, α-herpesvirinae, β-herpesvirinae, and γ-herpesvirinae, based primarily upon the cell types in which they replicate and establish latency.[4,5] The α-herpesviruses primarily replicate in mucosal epithelial cells and establish latency in peripheral neurons, while the other two subfamilies replicate and establish latency in primarily immune cells.[4] One of these α-herpesviruses, Herpes Simplex Virus 1 (HSV1), completely remodels host cell nuclear architecture by excluding chromatin to the periphery to make room for viral replication compartments (RCs) in a process known as Margination.[6] While Margination itself is a well-known phenomenon, the underlying mechanism of this process is not well understood.[6,7,8,9,10]

Here, we explore potential drivers of margination, including physical crowding out, biochemical packaging, or both working in tandem. The first possible mechanism for margination is simple steric hinderance from the increase of material within the nucleus as viral

proteins are translated and imported into the nucleus for virion assembly. As more and more material is crammed into the nucleus, less and less room remains for chromatin, so it is compressed against the inner surface of the nuclear envelope. The second possible mechanism for margination is that a viral protein or proteins activate a chromatin remodeling pathway or modify the activity of chromatin remodeling proteins so that the chromatin is gathered to the periphery of the nucleus in a well-organized manner. During this process, an increase in the total amount of heterochromatin would be likely. As these two processes are not mutually exclusive, the third possibility is that both mechanisms work in tandem to produce the margination observed during lytic infections.

To investigate the process of Margination we first selected GFP-K26 (kind gift from F. Homa, University of Pittsburgh) as the strain of HSV-1 to be used for all infections, and Vero cells as the host cells. GFP-K26 is a strain of HSV-1 with the capsomere protein K26 fluorescently labeled with GFP. Vero cells are African Green Monkey (*Cercopithecus aethiops*) kidney epithelial cells and are commonly used in the study of HSV-1. Next, we identified three time points of interest during a lytic infection to compare to mock infected cells – 2 hours post infection (hpi), 6hpi, and 10hpi. Then, we used a fluorescent particle tracking technique developed in our lab known as Sensors of IntraNuclear Kinetics (SINK) to measure chromatin mobility at these time points. Quantification of nuclear size and viral capsid intensity using fluorescence microscopy and image analysis helped us establish early (2hpi), intermediate (6hpi), and late (10hpi) time points during the HSV-1 replication cycle. SINK analysis of Mock infected, 2hpi, 6hpi, and 10hpi chromatin reveals that a reduction in chromatin motion occurs at every time point. Notably, the 2hpi time point precedes formation of viral RCs indicating that some biochemical pathway is reducing chromatin mobility before the possibility of steric

hinderance arises form RC formation. Interestingly, it has been shown previously that heterochromatin markers decrease and euchromatin markers increase in abundance as the infection proceeds.[11] This indicates that whatever the biochemical pathway being activated is, it is not the likely culprit, namely heterochromatinization. We would expect that a decrease in heterochromatin markers would result in an increase of chromatin mobility, however, SINK reveals the opposite. Our current hypothesis is that the reduction in heterochromatin markers increases compliance of the chromatin network making it more readily compressed by another as yet unknown force.

## Results

### Time Point Selection

To select the most informative time points to compare to mock infected cells we infected Vero cells with GFP-K26, then fixed the samples with formaldehyde after 2, 3, 4, 5, 6, 7, 8, 10, 11, 12, 13, and 14 hours. Cells were then stained for actin with rhodamine phalloidin and chromatin with Hoechst 33342. Images were taken at 63x magnification and with identical illumination settings. Images were analyzed using ImageJ to quantify the size of the nucleus and the intensity of the GFP-signal from viral particles. The full procedure is described in more detail in the Methods section, but a brief description will be included here. The Hoechst channel was thresholded so that nuclear area could be calculated. The thresholded Hoechst channel was then used as a mask to isolate GFP signal only from within nuclei in the GFP channel. The GFP signal was then measured as total intensity within the area of individual nuclei.

The average nuclear area and average capsid intensity per nucleus are plotted versus time after infection in Figure 5.1A. Neither value changes significantly for the first 3 time points

(2hpi, 3hpi, and 4hpi). 5hpi marks the point at which RCs first become visible and is also the point at which the first increase in the average size of the nuclei is detected. Capsid intensity peaks at 6hpi. Starting after 10hpi, both values fluctuate from time point to time point.

In Figure 5.1B the individual nuclear areas are plotted versus the individual capsid intensities. Most data points within a time point seem to cluster together with data points from the same time point. However, the 5hpi and 6hpi time points are not as tightly clustered. Furthermore, the earlier time points seem to form an early cluster (Figure 5.1G) as well as the later time points forming a late cluster (Figure 5.1I). The intermediate, 5hpi and 6hpi, time points that are not as tightly clustered seem to form a bridge between the two clusters (Figure 5.1H).

Figure 5.1C shows the center of mass (average of all nuclear area values within the time point plotted versus the average of all capsid intensity within the time point) of each of the individual time point clusters. The black line connects the points in chronological order to more easily show the change over time.

We selected a time point from each of these groups to represent the early, intermediate, and late stages of margination. Specifically, 2hpi represents the early stage of margination before RCs are visible; 6hpi represents the intermediate stage when RCs are growing and fusing together; and 10hpi represents the late stage after the RCs have fused to become a single RC encompassing the majority of the nuclear volume. Figures 5.1D-F show representative images of cells stained with Hoechst and Phalloidin and infected with GFP-K26 at each of these time points.

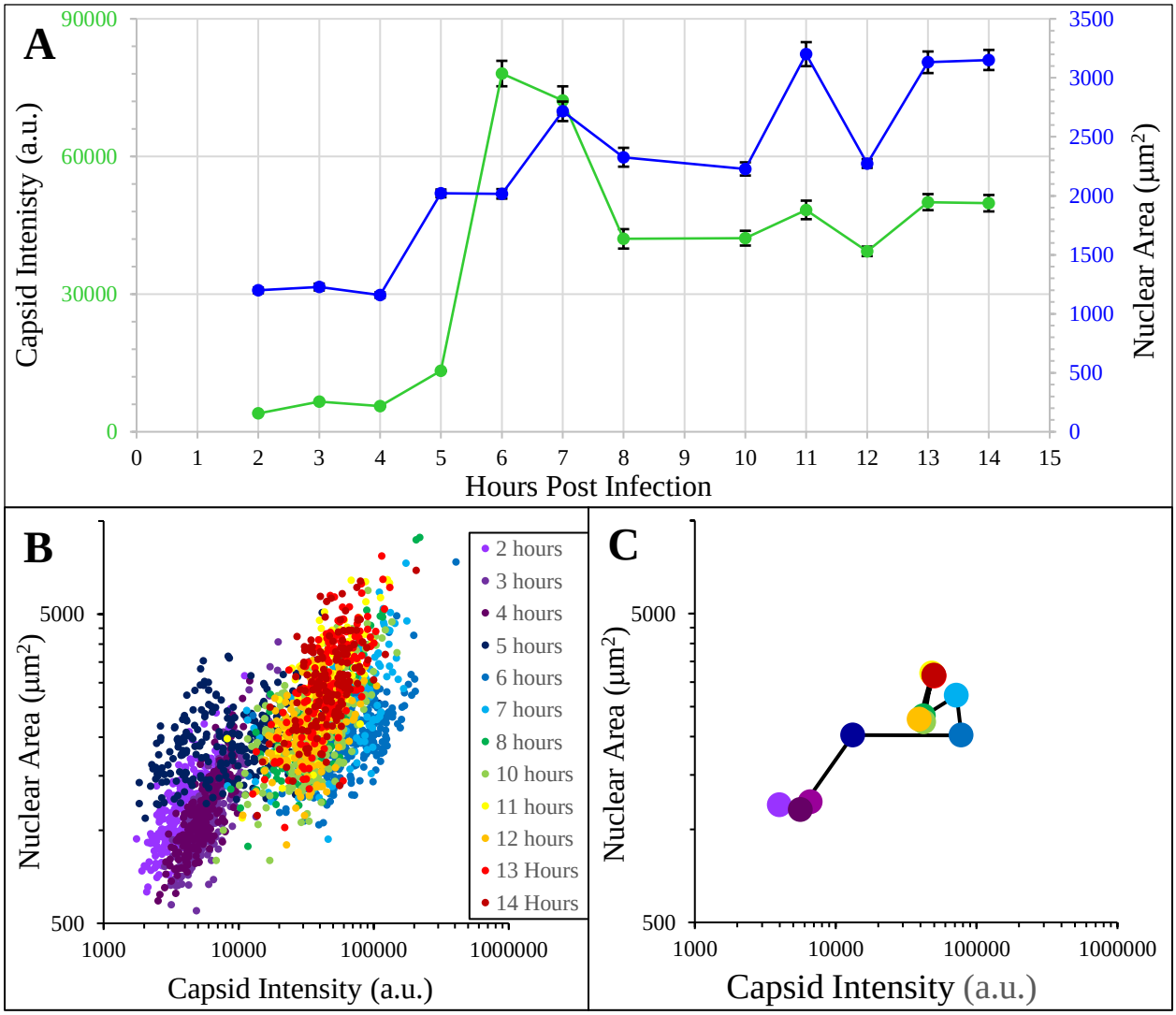
A
Capsid Intenisty (a.u.)
Nuclear Area (µm²)
Hours Post Infection
B
Nuclear Area (µm²)
Capsid Intensity (a.u.)
2 hours
3 hours
4 hours
5 hours
6 hours
7 hours
8 hours
10 hours
11 hours
12 hours
13 Hours
14 Hours
C
Nuclear Area (µm²)
Capsid Intensity (a.u.)

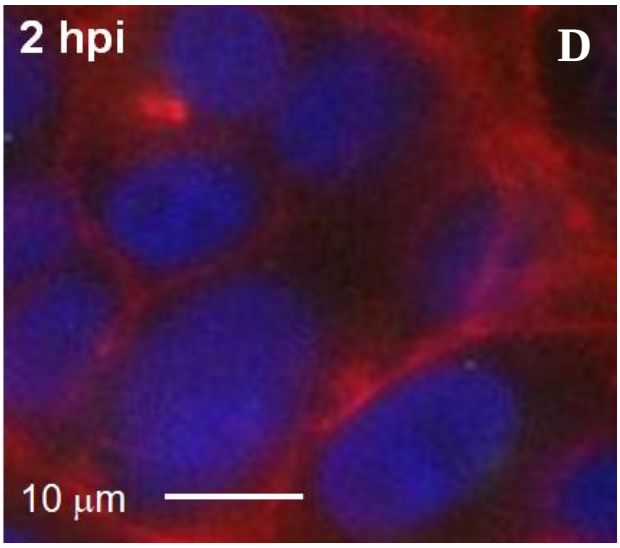
2 hpi
D
10 μm

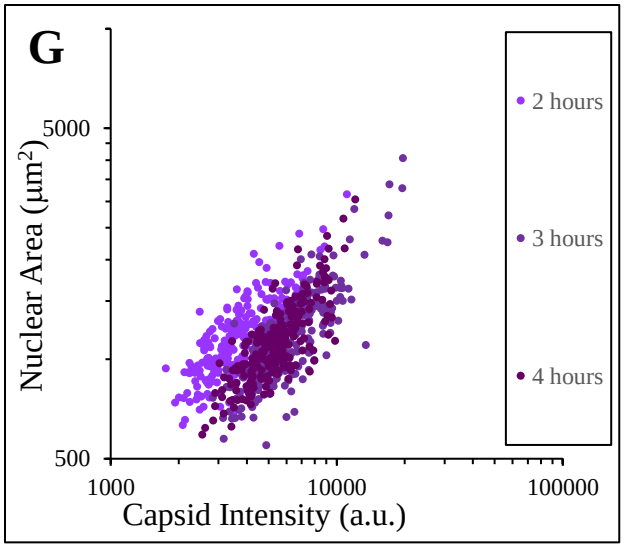
G
Nuclear Area (μm²)
5000
500
1000
10000
100000
Capsid Intensity (a.u.)
2 hours
3 hours
4 hours

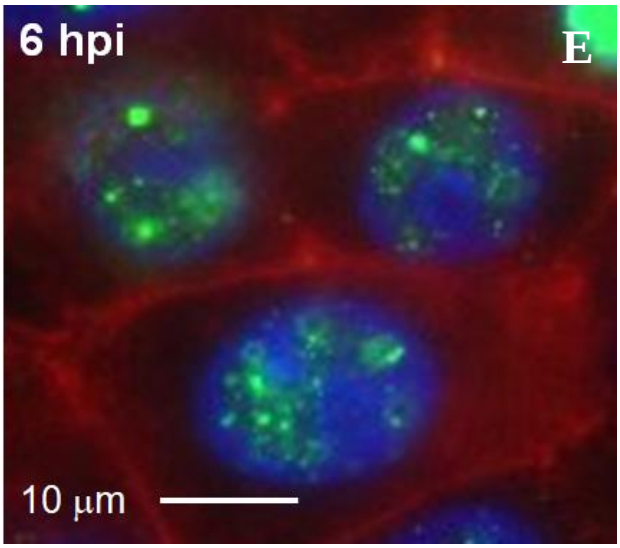
6 hpi
E
10 μm

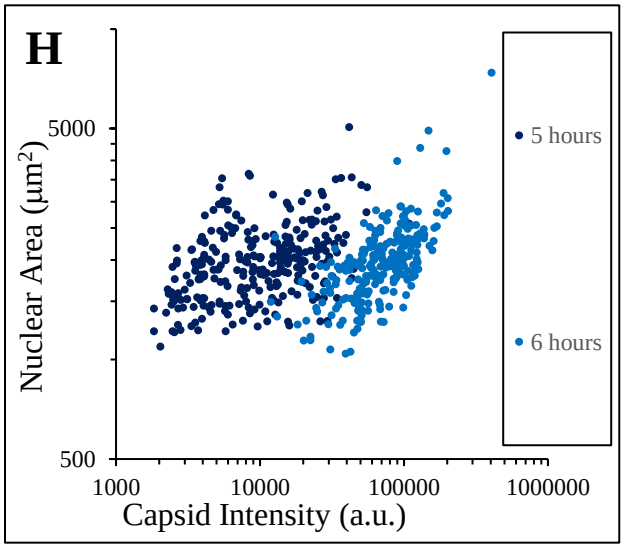
H
Nuclear Area (μm²)
5000
500
1000
10000
100000
1000000
Capsid Intensity (a.u.)
5 hours
6 hours

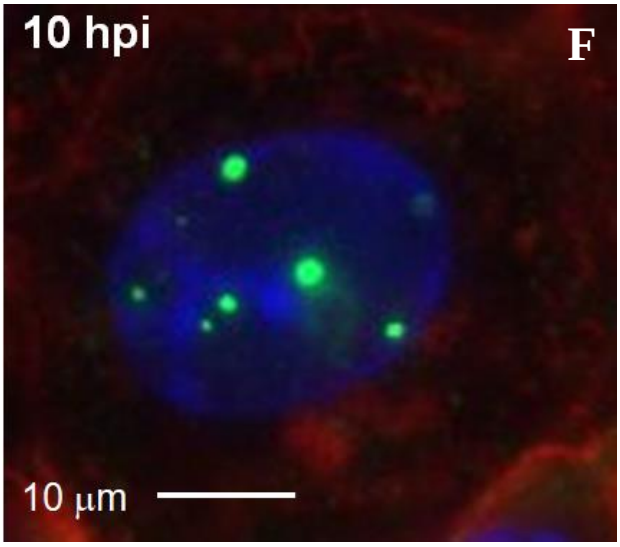
10 hpi
F
10 μm

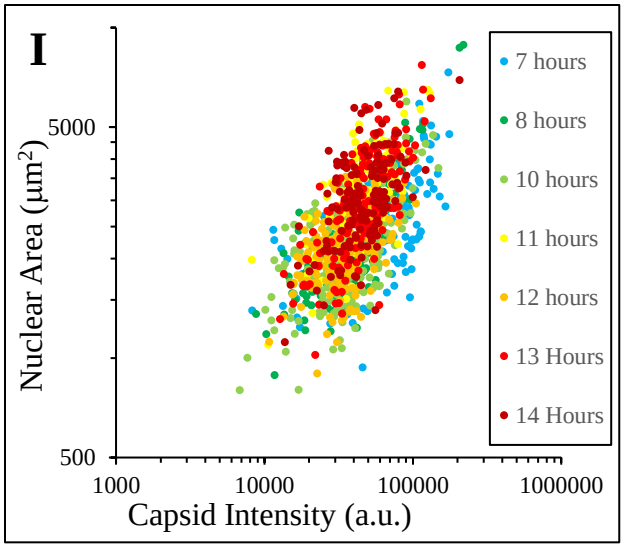
I
Nuclear Area (μm²)
5000
500
1000
10000
100000
1000000
Capsid Intensity (a.u.)
7 hours
8 hours
10 hours
11 hours
12 hours
13 Hours
14 Hours

***Figure 5.1: Line and scatter plots showing nuclear area and capsid fluorescence intensity at various time points throughout infection including representative fluorescence images of early, intermediate, and late time points. A)*** *Capsid Intensity (green) in arbitrary units (a.u.) and Nuclear Area (blue) in microns squared ($\mu m^2$) plotted versus hours post infection (hpi). Error bars are SEM. Number of cells analyzed per time point varies between time points from n=112 to n=281. The same cells were analyzed for both Capsid Intensity and Nuclear Area. Analysis completed using ImageJ.* ***B)*** *Scatter plot showing Capsid Intensity versus Nuclear Area. Each dot represents an individual cell. Colors represent time point as described in legend. Number of cells analyzed per time point varies between time points from n=112 to n=281. Total number of cells analyzed was 2377.* ***C)*** *Average Capsid Intensity versus Nuclear Area per time point. Colors represent time point as described in legend of B. Number of cells analyzed per time point varies between time points from n=112 to n=281. Total number of cells analyzed was 2377. Black line shows movement of the center of mass of the cluster through time.* ***D-F)*** *Representative images of cells at selected time points - 2, 6, and 10 hours post infection (hpi) respectively. Blue is Hoechst 33342 stain showing chromatin. Red is Rhodamine Phalloidin stain showing actin. Green is GFP-K26, a capsomere protein of HSV-1, showing viral replication centers. Scale bar is 10 microns.* ***G-I)*** *Scatter plots using the same data from B separated into Early, Middle, and Late time periods.*

## Chromatin Bound Probe Selection

Initially, Hoechst was used to stain chromatin. In previous studies, importantly ones utilizing SINK, in our lab, we used Hoechst with no serious drawbacks. However, previous studies did not involve infecting cells with a DNA virus. Since Hoechst stains DNA indiscriminately, the life cycle of the HSV-1 was negatively impacted by the DNA stain. Figure 5.2A shows the number of RCs that develop when DNA is stained with Hoechst. Figure 5.2B shows the same cells with GFP-K26 and Hoechst channels overlayed. Figure 5.2C shows how

many more replication centers form when the DNA is not stained by Hoechst. This was not a problem in the previous section where all staining occurred after fixation, but SINK requires live cell imaging. Therefore, an alternative chromatin bound probe had to be selected.

In previous studies we used chromatin bound probes such as Fibrillarin, TRF1, or UBF1 to mark specific structures within the nucleus. However, since HSV-1 reorganizes the entire nucleus, we did not know that these structures would survive the process of Margination. We decided to use a fluorescently tagged histone as a chromatin bound probe since we knew that at least some histones would always be bound to the DNA. Each of the four canonical histones has variants that are more common in certain structures or cell types than other variants. For example, H2A is replaced by H2AX (then phosphorylated to become γH2AX) near double strand breaks. We sought to avoid biasing our data toward the motion unique to one structure or region of the genome or another by selecting a canonical histone with few and rarely expressed variants. This also reduces the chance that this histone will be replaced with a variant as the cell responds to HSV-1 infection. H2B was selected since only a few variants exist and those are only expressed in a few highly specialized cell types that do not closely resemble the cell type used for SINK experiments.

The next step was selecting the fluorescent tag and delivery method. An RFP tag was used so as not to interfere with the GFP-tagged virions. A baculovirus vector was used to deliver the RFP-H2B. Since baculoviruses are insect viruses, all baculovirus genes have promoters designed for insect polymerases and are not transcribed by mammalian polymerases. Only the engineered RFP-H2B gene has a mammalian promoter. Therefore, the chance that the baculovirus vector interferes with any cellular or herpesviral process is minimal.

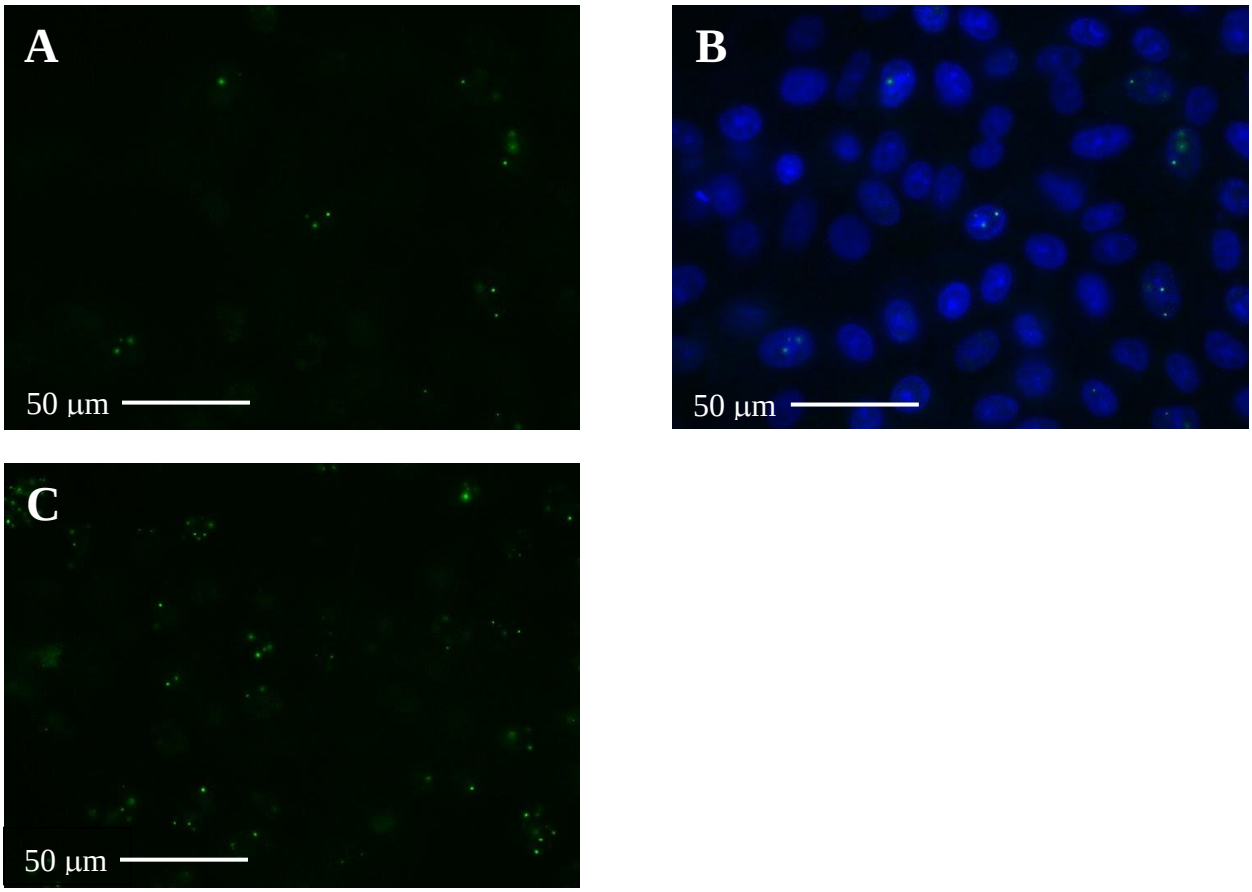


***Figure 5.2: Fluorescence images showing difference in viral replication with and without Hoechst DNA stain. A)*** *Representative image showing relative abundance of viral replication centers labeled with GFP-K26 when chromatin is stained with Hoechst during infection.* ***B)*** *Representative image showing overlay of GFP-K26 labeled replication centers with Hoechst marking chromatin.* ***C)*** *Representative image showing relative abundance of viral replication center labeled with GFP-K26 when chromatin is not stained with Hoechst during infection.*

**Chromatin Mobility Changes Throughout Infection**

In order to determine how the mobility of chromatin evolves throughout HSV-1 infection, we performed SINK analysis on mock infected Vero cells and Vero cells that were infected with GFP-K26 at 2hpi, 6hpi, and 10hpi. Vero cells were transfected using a baculovirus

vector with RFP-H2B to mark chromatin. Nuclei were imaged at 63x every 3 minutes for 1 hour in both green and red channels. Images were processed and analyzed and MSDs for both chromatin and viral particles were calculated as described in the Methods section. Figure 5.3 shows MSDs for RFP-H2B marked chromatin in Mock infected cells and cells 2hpi, 6hpi, and 10hpi. Unsurprisingly, Mock infected cells have the most mobile chromatin. Notably, the mobility of the chromatin has already decreased at 2hpi, which is before the formation of RCs of significant size or number. The trend of decreasing chromatin mobility continues through 6hpi and 10hpi. Since the decrease in mobility begins before the widespread formation of RCs it is likely that the process of Margination is not driven by a mechanism as simple as steric hindrance forcing chromatin to the periphery as new material is brought into the nucleus to assemble new virions.

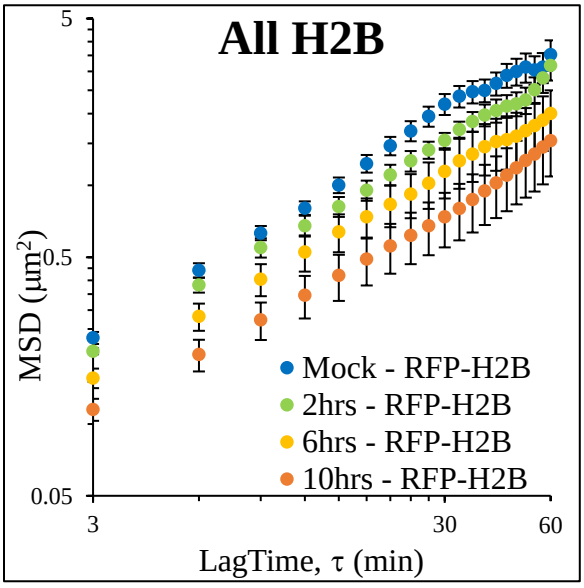


***Figure 5.3: Mean Squared Displacement plots showing reduction in chromatin mobility consistently throughout infection.*** *MSD of RFP-H2B marked chromatin in Mock infected cells (blue, n=10 cells, N=15 tracks), MSD of RFP-H2B marked chromatin in cells 2 hours post infection (green, n=6 cells, N=13 tracks), MSD of RFP-H2B marked chromatin in cells 6 hours post infection (yellow, n=21 cells,*

*N=56 tracks), MSD of RFP-H2B marked chromatin in in cells 10 hours post infection (orange, n=58 cells, N=249 tracks). Error bars are SEM.*

**Chromatin Mobility vs Viral Mobility**

Figures 5.4A-C show the relative mobility of chromatin and viral particles at 2hpi (Figure 5.4A), 6hpi (Figure 5.4B), and 10hpi (Figure 5.4C). Obviously, Mock infected cells are not included as there is no GFP-K26 signal in those cells. Interestingly, a few of the 2hpi cells did have GFP-K26 signal even though most cells did not develop RCs this early in the infection, a fact reflected in the low n value for the 2hpi – GFP-K26 MSD. The mobility of the viral particles seems to decrease more quickly than the mobility of the chromatin as indicated by the wider gap between the chromatin and viral MSDs at 6hpi than at 2hpi. In Figure 5.4D, we can see that there is no decrease in viral particle motion between 6hpi and 10hpi. This is likely because these viral particles are enmeshed into the larger RC and the motion of these particles is actually the motion of the entire RC. This much larger structure within the nucleus would certainly be less mobile than the much smaller and independently mobile early RCs measured at 2hpi.

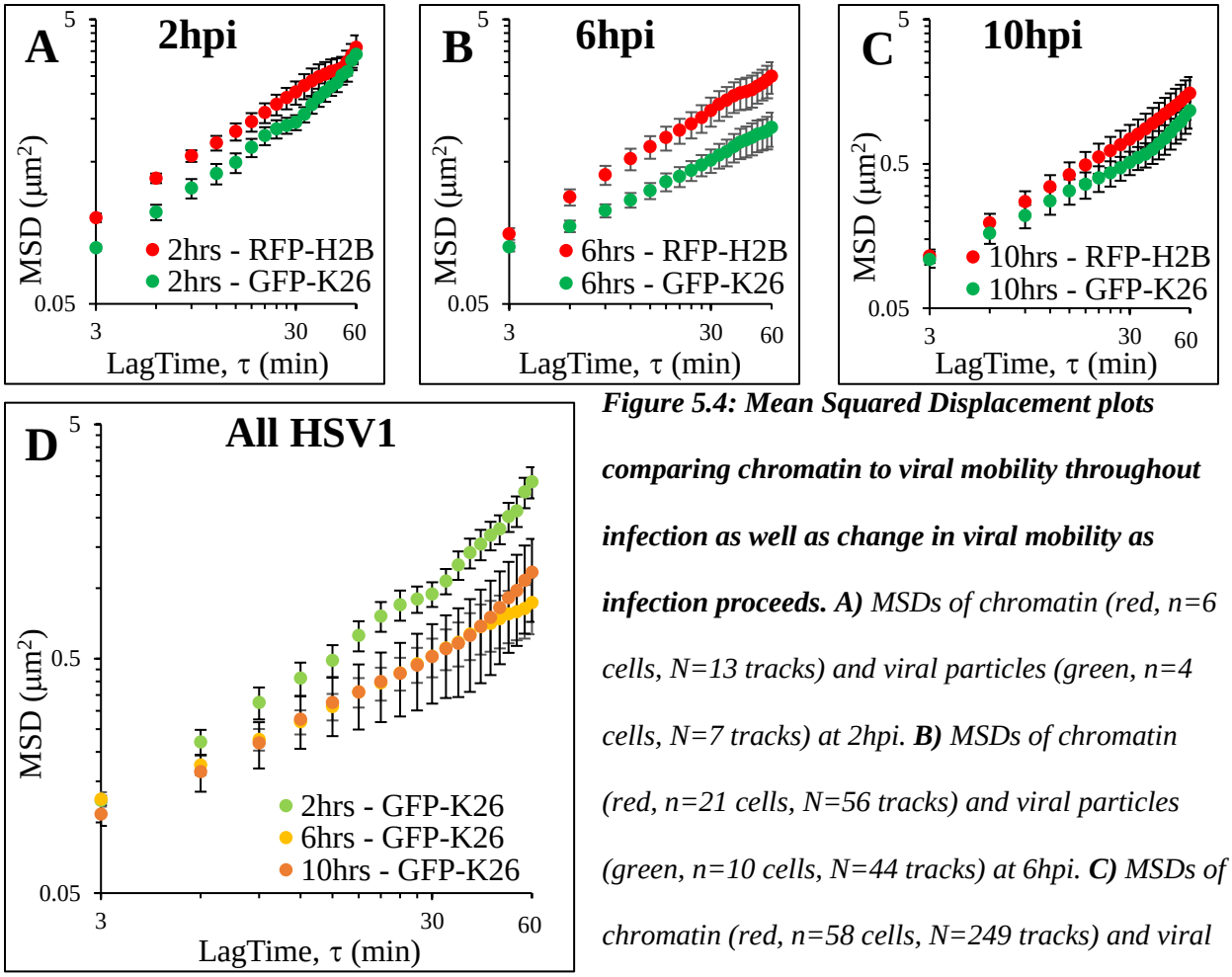


***Figure 5.4: Mean Squared Displacement plots comparing chromatin to viral mobility throughout infection as well as change in viral mobility as infection proceeds. A)*** *MSDs of chromatin (red, n=6 cells, N=13 tracks) and viral particles (green, n=4 cells, N=7 tracks) at 2hpi.* ***B)*** *MSDs of chromatin (red, n=21 cells, N=56 tracks) and viral particles (green, n=10 cells, N=44 tracks) at 6hpi.* ***C)*** *MSDs of chromatin (red, n=58 cells, N=249 tracks) and viral particles (green, n=38 cells, N=110 tracks) at 10hpi.* ***D)*** *Viral particle mobility at 2hpi (green, n=4 cells, N=7 tracks), 6hpi (yellow, n=21 cells, N=56 tracks), and 10hpi (orange, n=38 cells, N=110 tracks) compared.*

## Discussion

The process of Margination, even though often observed, remains largely unexplained. It is clear that Margination is driven by some mechanism initiated by HSV-1 infection, but the exact nature of this mechanism continues to elude researchers. Here, we begin to explore this mystery by comparing chromatin mobility at various time points throughout infection to observations of the formation of viral replication compartments at the same time points. As

global chromatin mobility decreases significantly before the appearance of viral RCs we can rule out the possibility of a simple mechanism of molecular crowding out purely through the action of steric hindrance as materials are imported into the nucleus to assemble new virions. This evidence indicates that HSV-1 is initiating some type of chromatin remodeling mechanism preceding formation of viral RCs. This mechanism may be solely mediated by viral proteins expressed in the first 2 hours of infection, or may be due to certain cellular proteins or entire pathways being activated by viral proteins. Perhaps the most obvious cellular pathways to investigate would be pathways that increase heterochromatin levels as these would increase the amount of condensed heterochromatin, the majority of which is already at the periphery of the nucleus. However, findings from Kulej, Molecular & Cellular Proteomics, 2017 show decreased expression of heterochromatin markers and increased expression of euchromatin markers.[11] More investigation is certainly necessary. ChIP-seq would be quite useful in not only discovering which hetero- or euchromatin markers are increased or decreased in expression levels, but where in the genome these changes are occurring. It may be that certain areas are being amplified in heterochromatin markers, but in other areas the heterochromatin markers are being removed. Kulej, Molecular & Cellular Proteomics, 2017 only reported net changes to global expression, not the local resolution that ChIP-seq would provide.

## Methods

### Cell Culture

Vero cells were cultured in DMEM high glucose media supplemented with 10% FBS and 1% penicillin-streptomycin (Life Technologies, Grand Island, NY). During passaging cells were

trypsinized with 0.25% Trypsin-EDTA with phenol red (Thermo Scientific, Waltham, MA) and neutralized with FBS-containing culture media.

**Transfection**

Vero cells were passaged into 35 mm ibiTreat μ-dishes (ibidi, Fitchburg, WI) and transfected with BacMam 2.0 RFP-H2B (Invitrogen, Waltham, MA). Cells were then returned to the incubator for between 24 and 48 hours before experiments were run to allow widespread expression of RFP-H2B.

**HSV-1 Infection**

Media was aspirated and cells were rinsed with PBS to remove debris. 200 μL of cold media straight from 4°C refrigerator was pipetted carefully into only the inner well of the 35 mm ibiTreat μ-dishes. GFP-K26 was added to cells at 10 MOI and sealed dish was placed in a box containing a damp paper towel to prevent evaporation. Box was placed into 4°C refrigerator for 1 hour. After 1 hour, 2 mL of 37°C media was added to imaging dishes which were then placed in incubator for 2, 6, or 10 hours depending on the experiment being run. The same procedure was followed for Mock infected cells minus adding GFP-K26. After warm media was added, Mock infected cells were imaged.

The reason for placing cells in the refrigerator after infection has to do with viral attachment and entry into cells. Attachment is energy independent and so will occur at 4°C. The lower volume of media speeds up this process as particles have a smaller volume to diffuse through before they come into contact with cells. Entry into cells, however, is energy dependent,

meaning that entry only occurs at body temperature. These steps ensure simultaneous infection and synchronize the infection cycle in all cells in the dish.

**Particle Tracking**

Imaging for particle tracking experiments was done using a 63x, 1.4 NA, oil immersion objective of an inverted microscope (DMI6000, Leica, Buffalo Grove, IL) in a controlled live-cell imaging chamber with humidified 5% $CO_2$ and held at 37 °C. Images were taken at multiple (8–12) positions per plate at 3-minute intervals with multiple transfected cells per field of view and multiple particles per cell. Cell cycle was not arrested due to possible alterations in gene expression that could bias results. Instead, cells were inspected after imaging was complete to ensure cells showed no signs of mitosis or apoptosis. Two-dimensional tracking of RFP-H2B chromatin regions and GFP-K26 viral particles was performed using custom Laptrack71 programs designed in MATLAB (Natick, MA) as previously published.[12] Briefly, images were cropped and aligned to remove artifacts including imaging drift, nuclear translation, and nuclear rotation. Therefore, only intranuclear motion of particles was tracked. Particles were then detected through statistical algorithms after calibration of background noise parameters. Particle tracks were then determined by correspondence with succeeding frames. Only persistent tracks of particles present for the full duration of the experiment were used for further analysis. The ensemble-averaged MSD was calculated from the particle tracks as shown in the equation $MSD(\tau) = \langle (x_{\tau+3} - x_\tau)^2 + (y_{\tau+3} - y_\tau)^2 \rangle$, where $\tau$ is the lag time.

Outliers, defined as tracks which were greater than 3 standard deviations away from the ensemble average at the final lag time, were removed from the dataset. The ‘n’ values reported in figure legends represent the number of cells analyzed. The ‘N’ values reported in figure legends

represent the number of tracks analyzed. MSD magnitudes were compared at each time point using Student's t-test. Error bars on MSD plots represent Standard Error of the Mean.

**Fixing and Staining**

Cells grown and infected in 35mm ibiTreat m-dishes (ibidi, Fitchburg, WI) were fixed with 3.7% formaldehyde for 15 minutes, then rinsed 3 times with 1X PBS. Cells were permeabilized with 0.2% Triton X-100 for 15 minutes, then rinsed 3 times with 1X PBS. Cells were blocked against non-specific binding with 0.2% BSA for 1 hour, then rinsed 3 times with 1X PBS. Simultaneously, Rhodamine Phalloidin (Invitrogen, Waltham, MA) and Hoechst 33342 (Life Technologies, Grand Island, NY) were diluted in 0.2% BSA and used to label cells for 1 hour while being protected from light, then rinsed 3 times with 1X PBS. The third rinse with 1X PBS was left in the 35mm ibiTreat m-dish for storage and imaging.

## References


1. Flint, S. J., Racaniello, V. R., Rall, G. F., Skalka, A. M., & Enquist, L. W. Principles of Virology 4th Ed. 514 (ASM Books, 2015).
2. Carter, J., Saunders, V. Virology, Principles and Applications 2nd Ed. 121-134 (Wiley, 2013).
3. Hu M. Y., Depledge D. P., Cortes E. F., Breuer J., & Schang L. M. Chromatin dynamics and the transcriptional competence of HSV-1 genomes during lytic infections. *PlosPathogens*. **15**, 1-37 (2019).
4. Grinde B. Herpesviruses: latency and reactivation – viral strategies and host response. *Journal of Oral Microbiology*. **5**, 1-9 (2013).
5. Davison A. J. et al. The Order Herpesvirales. *Arch Virol*. **154**, 171-177 (2009).
6. Simpson-Holley M., Colgrove R. C., Nalepa G., Harper J. W., & Knipe D. M. Identification and Functional Evaluation of Cellular and Viral Factors Involved in the Alteration of Nuclear Architecture during Herpes Simplex Virus 1 Infection. *Journal of Virology*. **79**, 12840-12851 (2005).
7. Monier K., Armas J. C. G., Etteldorf S., Ghazal P., & Sullivan K. F. Annexation of the interchromosomal space during viral infection. *Nature Cell Bio*. **2**, 661-665 (2000).
8. Weller S. K. Herpes Simplex Virus Reorganizes the Cellular DNA Repair and Protein Quality Control Machinery. *PlosPathogens*. **6**, 1-3 (2010).

9. Bosse J. B., Hogue I. B., Feric M., Thiberge S. Y., Sodeik B., Brangwynne C. P., & Enquist L. W. Remodeling nuclear architecture allows efficient transport of herpesvirus capsids by diffusion. *PNAS*. E5725-E5733 (2015).
10. Flomm F. & Bosse J. B. Potential mechanisms facilitating herpesvirus-induced nuclear remodeling: how are herpesvirus capsids able to leave the nucleus? *Future Virology*. 1-10 (2017).
11. Kulej K., Avgousti D. C., Sidoli S., Herrmann C., Fera A. N. D., Kim E. T., Garcia B. A., & Weitzman M. D. Time-resolved Global and Chromatin Proteomics during Herpes Simplex Virus Type 1 (HSV-1) Infection. *Molecular & Cellular Proteomics*. **16**, S92-S107 (2017).
12. Booth-Gauthier E. A., Alcoster T. A., Yang G. & Dahl K. N. Force-induced changes in subnuclear movement and rheology. *Biophys. J.* **103**, 2423-2431 (2012).

# Chapter VI

## Epigenetic Changes During Mechanical Stress

The Wickstrom Lab at the University of Helsinki sought our expertise in measuring chromatin motion to study how cells are able to protect their genome from mechanical stress. They showed that nuclear deformation triggered an influx of intracellular $Ca^{2+}$ to the cytoplasm which led to reduced methyltransferase activity and thus decreased the amount of H3K9me3 marked heterochromatin. Our contribution showed that chromatin mobility, measured by SINK, was increased when cells were stretched for 30 minutes. We also showed using SINK that this increase in chromatin mobility was transient, as the mobility of chromatin in cells stretched for 6 hours was statistically indistinguishable from that of unstretched cells. This finding fit well with an additional finding of the Wickstrom Lab that cell monolayers reoriented over longer stretch times to reduce stress upon each nucleus.

### Summary of Nava et al., Cell, 2020

This paper, Heterochromatin-Driven Nuclear Softening Protects the Genome against Mechanical Stress-Induced Damage, begins with the observation that many epithelial tissues undergo large-scale mechanical deformations and are subjected to significant amounts of mechanical stress, but do not develop persistent DNA damage lesions to the same extent that cancer cells do under similar levels of mechanical deformation and stress. Nava et al. found that chromatin quickly responds to mechanical stress to prevent DNA damage, then the cytoskeleton, which undergoes remodeling at a slower rate, reorients to protect the nucleus from mechanical stress and allow chromatin to return to its resting state.

In the first set of experiments, Nava et al. subjected epithelial monolayers to cyclic (at 100 mHz) stretch at 5%, 20%, or 40%. In general, changes noted at 5% stretch were more subtle but also more persistent, while changes at 40% were more drastic but more transient, and changes at 20% stretch seemed to be intermediate. The specific changes observed were to the shape and orientation of the nucleus, actin fibers in the cytoskeleton, and the amount of heterochromatin markers. At 40% stretch the nucleus elongated, flattened, and aligned perpendicular to the direction of the stretch, while 5% stretch did not induce any of these changes. At both 5% and 40% stretch perinuclear actin formed to stabilize the nucleus but was more persistent at 5% and more transient at 40%. At 40% stretch the actin cytoskeleton realigned facilitating the full monolayer of cells to align perpendicular to the direction of the stretch. 20% stretch induced alignment to a lesser degree. However, at 5% stretch no alignment occurred. Changes observed in heterochromatin markers were most apparent in K3K9me3. In the first 30 minutes of stretch H3K9me3 levels decreased for both 5% and 40% stretch, however, at 40% stretch these levels had recovered after 3 hours while the H3K9me3 levels were still depleted after 6 hours for 5% stretch. These findings indicate that the response is amplitude sensitive, and that the higher amplitude response has a rapid but transient early mechanism involving the nucleus and a slower but more persistent late mechanism involving the actin cytoskeleton.

Next, a closer look was taken at the changes to chromatin in cells stretched at 40%. Using ChIP-seq it was determined that the regions losing H3K9me3 marked heterochromatin were mainly non-coding sequences of DNA, often towards the ends of chromosomes, that tended to be at the periphery of the nucleus close to the lamina. The transcriptome of these cells was also analyzed revealing relatively few genes being differentially expressed. Of these, the genes that had increased expression were mostly related to cell-cell junctions, the cytoskeleton, and

heterochromatin regulation, while the genes that had decreased regulation were mostly related to epithelial differentiation.

Since the transient changes observed during the 40% stretch experiments occurred either just inside or just outside of the nuclear envelope, nuclear mechanical properties, specifically tension, were investigated further. Superresolution microscopy revealed that the nuclear envelope was wrinkling. Similar to the previous experiments, this occurred to a lesser degree but was more persistent after 5% stretch and occurred to a greater degree but more transiently after 40% stretch. Nuclear wrinkling is usually a sign of decreased nuclear membrane tension and increased deformability, both of which were confirmed by AFM. Further support for a decrease in nuclear membrane tension and an increase in nuclear deformability was provided by FLIM experiments as well. Interestingly, depolymerization of actin did not alter the wrinkled state of the nuclear envelope indicating that the perinuclear actin was not the cause of the wrinkling.

To determine if the decrease in heterochromatin was the cause of the nuclear envelope wrinkling and whether this actually had the effect of preventing DNA damage as hypothesized, the role of a methyltransferase (Suv39H1) known to be down regulated after 40% stretch was studied in more detail. Suv39H1 was overexpressed in 40% stretched cells. This prevented the previously observed decrease in H3K9me3 and also nuclear softening. Inhibition of Suv39H1 also led to a decrease in H3K9me3 and nuclear stiffness in unstretched cells. These findings indicate that the reduction in tension and wrinkling are the result of decreased H3K9me3 due to down regulation of Suv39H1. To further validate this conclusion, SINK was used to directly measure the stiffness of the chromatin in unstretched cells, in cells stretched for 30 minutes at 40%, and in cells stretched for 6 hours at 40%. SINK revealed increased chromatin mobility, indicating less stiff chromatin, after 30 minutes of 40% stretch, but after 6 hours, similar to the

previous experiments, chromatin mobility had decreased to match the unstretched chromatin mobility again, indicating that this change in chromatin was transient like the previous changes observed in cells stretched at 40%. To determine if these changes actually serve to prevent DNA damage, γH2AX foci were quantified in stretched cells with and without Suv39H1 overexpression. More DNA damage was detected in cells overexpressing Suv39H1 that did not have decreased H3K9me3 levels indicating that softening of the chromatin and nuclear envelope does in fact play a role in DNA damage prevention.

The next question to answer in this investigation was 'What induces the down regulation of Suv39H1?' First α-catenin was studied because it is known to play a role in mechanotransduction, and it is found in adherens junctions known to be altered by stretch. Inhibition of α-catenin prevented actin and monolayer alignment, but not the changes to chromatin and the nuclear envelope, indicating that α-catenin played a role in the cytoskeletal process, but not the chromatin process. Another possibility was $Ca^{2+}$ signaling as imaging had confirmed increased $Ca^{2+}$ levels in the cytoplasm. Using $GdCl_3$ to inhibit stretch-induced $Ca^{2+}$ channels prevented the chromatin process but not the cytoskeletal process indicating that the two processes are distinct from initiation to effect and not just branching effects of the same mechanism. Next, a specific $Ca^{2+}$ channel was investigated, Piezo1. Inhibition of Piezo1 prevented the changes to chromatin from occurring. To determine the source of cytosolic $Ca^{2+}$ experiments were run depleting $Ca^{2+}$ within the ER and chelating $Ca^{2+}$ inside the cells. Both experiments prevented the changes to heterochromatin previously observed. Removing extracellular $Ca^{2+}$ failed to prevent these changes to heterochromatin indicating that the reservoir of $Ca^{2+}$ being drawn upon by this process is the $Ca^{2+}$ in the ER. The cytoskeletal process,

however, does rely on extracellular $Ca^{2+}$ as it relies on adherens junctions which rely on $Ca^{2+}$ to form.

To further investigate the interplay between nuclear envelope tension and $Ca^{2+}$ release two stem cell types, EPCs and MSCs, which generally have high nuclear envelope tension, and two cancer cell lines, SCC9 and HT1080, which generally have low nuclear envelope tension were stretched as before at 40%. The stem cell types were able to reduce H3K9me3 and the cancer cell lines were not. However, when the Lamin A levels in the HT1080 cells were increased by overexpression, H3K9me3 was reduced, and similarly, when Lamin A was knocked down by siRNA in EPCs H3K9me3 did not decrease. These experiments show that a minimum threshold of nuclear envelope stiffness is necessary for this mechanism to trigger.

To determine if the transient nature of the chromatin and nuclear softening was due to nuclear strain being decreased by the cytoskeletal realignment monolayers were pre-stretched at 40% for 6 hours, stretched again either along the same axis of stretch or perpendicular to the pre-stretch. Monolayers stretched in the same direction did not alter their heterochromatin structure as before, indicating that the realignment of the cytoskeleton during the pre-stretch was already protecting the genome from damage. Monolayers stretched perpendicular to the pre-stretch underwent the same processes of heterochromatin rearrangement and cytoskeletal realignment as previous experiments, indicating that the genome required other means of protection while the cytoskeleton was realigning.

Finally, to validate results in a more natural system, similar stretch experiments were run and H3K9me3 levels analyzed using intact skin from mouse embryos. Similar results were observed using *ex vivo* intact skin indicating that the conclusions reached translated beyond the more idealized systems of monolayers *in vitro*.

## Description of my contribution

This author's contribution to Nava et al., Cell, 2020 was to perform SINK analysis on image sequences provided by the Wickstrom lab. These sequences were of the nuclei of single epidermis stem/progenitor cells (EPC) under three conditions: in a monolayer with no stretching, in a monolayer after 30 minutes of 40% stretch, and in a monolayer after 6 hours of 40% stretch. The chromatin bound probe used was TRF1, a telomeric protein, labeled by CRISPR-Rainbow, a system for labeling specific sequences of DNA using sgRNA and the inactive nuclease dCas9.

The data from this SINK analysis fit well with the rest of the data published in Nava et al., Cell, 2020. After 30 minutes of stretch the chromatin has become softer and more mobile (for Lag Times less than 2 minutes at least), and after 6 hours once the cytoskeletal realignment has had time to finish, the stress has been removed from the nucleus and the chromatin returns to its baseline level of mobility. This was confirmed by running a Student's t-test at every Lag Time with a 99.9% confidence interval. An interesting result not discussed in great detail in the published paper was the irregular shape of the MSD plot for the cells after being stretched for 30 minutes at 40%. At Lag Times less than about 2 minutes the mobility of the chromatin in these cells is greater than the other conditions. However, in Lag Times of longer than 2 minutes (with the change in trajectory occurring at a Lag Time of about 90 seconds) the mobility of the chromatin in these cells seems to be less than the baseline mobility. The shape of this data seems to indicate caged motion. A phenomenon in which the mobility of the chromatin increases as the chromatin becomes softer and softer, but at a certain point the mechanical properties of a larger structure, for instance chromatin or the nuclear membrane itself, limit the mobility in a similar way to a cage restricting motion outside of its boundaries. Precisely what structure is leading to

this caged motion behavior and why it does not affect the baseline motion of the chromatin will require further study to determine.

Unlike SINK experiments in the previous project described in this work, these sequences were not generated by taking images every 3 minutes for 1 hour. These sequences were generated by taking images every second for 3 minutes. This required me to read, understand, modify, and troubleshoot the source code of certain programs within the MatLab suite the Dahl lab uses to analyze SINK data. The number of frames was the main concern, and to a lesser extent the pixel to micron ratio. Altering the pixel to micron ratio required only an email exchange with the researcher in Helsinki that actually took the images to make sure of the new ratio and a quick edit in a few programs that are commonly edited each experiment anyway so that the program knows where to find the data of interest for each new experiment. To change the frame length, however, required reprograming certain programs that were not the usual programs that get edited each experiment, but ones that are usually saved in a particular place and all but forgotten about. These programs were hard coded to expect 21 frame sequences and took careful, line-by-line reading of the code to ensure any, every, and only lines that were written to handle 21 frame movies were changed, so as not to cause any errors. The change from an interval of 3 minutes to 1 second was the easiest change, requiring only a change of axis label.

Another challenge to completing the SINK analysis for this project was a matter of processing power. The MatLab suite that the Dahl lab uses runs quickly enough when processing movies of only 21 frames. When the movies being analyzed are nearly 9 times the frame length the analysis takes much longer.

## Discussion

Overall, Nava et al., Cell, 2020 validates the robustness of the SINK method in multiple ways. This article shows that SINK data is consistent with many other non-mechanical methods more traditionally used in biology. The data also adds motion to the mental image in the researcher's mind of the process being investigated that more traditional methods do not provide. Another way that this article has validated SINK's robustness is that it has shown the flexibility that SINK has in being modified to fit a certain application. Here specifically, that experiment length and imaging frequency are not locked into the standard 1 hour length and 3 minute imaging frequency.

## Reference

1. Nava et al. Heterochromatin-Driven Nuclear Softening Protects the Genome against Mechanical Stress-Induced Damage. *Cell*. **181**, 800-817 (2020).

# Chapter VII

## Conclusions

### Summation and Conclusions

The study of chromatin motion at many scales and under many forms of perturbation will continue to be important. This research has shown the versatility of the SINK method in studying genomic insults at multiple scales and conditions, from site-specific differences between heterochromatin and euchromatin, to global DNA damage after drug treatment, to global reorganization due to viral infection. In combination with other methods, SINK helped to elucidate how cells protect their genome from mechanical stress. Overall, this research shows that SINK has an important role to play in the study of chromatin insults because of its versatility in application and the usefulness as an orthogonal approach.

In Chapter II we introduced the SINK method. The power of SINK is its adaptability to a variety of applications. Any adherent eukaryotic cell type may be analyzed using SINK. The lengths of experiments and the interval between frames may be tailored to fit the process a researcher is trying to study. Perhaps the most customizable part of SINK is the chromatin bound probes. Researchers may stain the DNA itself with Hoechst to measure bulk motion of the chromatin or focus on specific structures such as nucleoli or telomeres with proteins such as Fibrillarin or TRF1 or even specific sequences within the genome if a protein with a specific binding motif is used as in Chapter III. This work is intended to serve as an example of the diversity in experimental contexts in which SINK may be employed to spark creativity and inspire other researchers make their own discoveries using SINK.

Reactive Oxidative Stress is an inescapable threat to genome integrity since the Reactive Oxygen Species responsible are generated within the cell's own mitochondria. ROS can cause a variety of DNA lesions including double strand breaks, which can alter the local mechanical properties of the chromatin network. In Chapter III we examined the differences in the DNA damage response to these lesions in two distinct chromatin structural regimes. First, we showed that the bulk chromatin motion could be measured with any chromatin bound probe with foci dispersed throughout the nucleus. Then, we compared the motion of highly specific foci in either a euchromatin regime or a heterochromatin regime to this bulk average which was measured by fibrillarin dispersed throughout the nucleus in various nucleoli. Euchromatin foci displayed similar mobility to the bulk average while heterochromatin was unsurprisingly less mobile. Chromatin mobility was measured at these distinct genomic locations again after damage had been induced by ROS and no change in the relative mobility of euchromatin as compared to the bulk average was observed, however, the mobility of the heterochromatic region had increased so that it was also similar to the bulk average. Allowing additional time from the initiation of damage in the euchromatin region we measured the mobility again. For shorter Lag Times the motion of the damage foci was greater than the bulk average but similar to the motion of damage foci, marked by 53BP1, that develop after genome-wide treatment with bleocin. At longer Lag Times the MSD plot becomes erratic suggesting high variability from several competing processes. In the end, this study highlights how chromatin mobility evolves over time and suggests that an extra mobilization step may be required for damage repair to proceed in heterochromatin. This study also highlights the specificity that SINK is capable of, in that specific sequences of DNA were targeted for measurement as well as specific structures throughout the nucleus such as the damage foci marked by 53BP1.

If new and more powerful chemotherapy drugs are to be developed, then understanding why existing drugs are effective is vital. In Chapter IV, we begin to identify differences between a cisplatin sensitive cell line and other cell types including healthy breast epithelial cells. Using SINK, we discovered differences in the mechanical response of chromatin to cisplatin treatment between cell types that are not particularly sensitive to cisplatin and one that is. First, we established the baseline chromatin mobility in all four cell types by performing SINK on untreated cells. Next, we showed that the healthy response to cisplatin treatment is a general stiffening of the chromatin network by treating healthy primary hMEC cells with cisplatin and measuring chromatin mobility. Chromatin in non-sensitive cancer cell lines, HCC1806 and Hs578T, displayed similar stiffening after cisplatin treatment. The same stiffening of the chromatin network was not observed in cisplatin sensitive MDA-MB-231 cells suggesting the potential that sensitivity arises from an inability to effectively exert control over chromatin architecture in the event of cisplatin induced DNA lesions. To ensure that damage was in fact occurring and that the lack of change in chromatin mobility was not due to an absence of damage, MDA-MB-231 cells were stained for γH2AX. More γH2AX foci were visible in MDA-MB-231 cells than the healthy hMECs, and when treated with a dose 10x higher the cisplatin sensitive cells showed a corresponding increase in γH2AX foci. As the MSD plots of all four cell types displayed scale invariant behavior, we were also able to glean more biophysical data from the SINK experiments by fitting the data to a power law. The lack of change in β between the untreated and cisplatin treated MSDs for any of the cell types indicates that the reduction in chromatin mobility, or the lack thereof, is not related to force propagation through the chromatin network. The decrease in the $D_{eff}$ value of the three cell types not particularly sensitive to cisplatin, and the lack of decrease in the $D_{eff}$ value of the cisplatin sensitive cells indicate that the

particular property of chromatin architecture that MDA-MB-231 cells are not able to properly exert control over is their chromatin condensation state. Beyond the specific findings, this study has demonstrated that SINK is a powerful tool in zeroing in on likely mechanisms responsible for a particular phenomenon of interest.

In Chapter V we sought to explore a well-documented but understudied phenomenon in virology. Although it has been observed and documented in many studies before, very little work has been done to define the mechanism of margination in HSV-1 infected cells. In this work, we began with a very high altitude question: Is margination primarily a mechanical process driven by steric hindrance, or primarily a biological process driven by the activation of a chromatin packaging pathway? Based upon the quantification of changes to nuclear area and the intensity of GFP-tagged viral capsids, we selected three time points during the infection cycle to focus upon: an early time point at 2hpi that precedes the formation of visible replication centers, an intermediate time point at 6hpi that coincides with RCs beginning to fuse together, and a late time point at 10hpi when the RCs have completely remodeled the internal architecture of the nucleus. Measuring chromatin mobility at these time points as well as in mock infected cells using SINK revealed that chromatin mobility starts to be restricted as early as 2hpi. As RCs have not yet begun to form at 2hpi, and thus not enough extra material has been imported into the nucleus to lead to more restricted chromatin motion, this finding suggests that margination is driven by the activation of some chromatin remodeling pathway and not simply steric hindrance. Further examination revealed that viral particles at 2hpi were more mobile than later time points, and that at the later time points, 6hpi and 10hpi, the motion of viral particles is nearly identical. Likely, at 2hpi the few viral particles able to be observed are isolated and can move independently of each other, while at later time points the viral particles are enmeshed in RCs

that have begun to merge so that motion is both coherent and restricted. Overall, this study exemplified the power of SINK in distinguishing between a mechanically driven phenomenon and a biologically driven phenomenon with downstream mechanical effects.

In previous chapters we exhibited how SINK may be used as the primary tool in studying a mechanical phenomenon, however, Chapter VI exemplifies how SINK can supplement more traditional methods to add depth and motion to the mental image being painted. Nava et al., Cell, 2020 described how the genome is protected from mechanical stress induced DNA damage by a fast acting chromatin structural response that is gradually then replaced by a slower acting cytoskeletal response that allows the chromatin to return to its resting state. Using SINK, we were able to show that the changes to the epigenetics of the chromatin and the mechanical properties of the nucleus as a whole were directly related to changes in chromatin motion. Specifically, we were able to directly measure that chromatin mobility increased as H3K9me3 marks were depleted, and nuclear envelope tension decreased. Similarly, as H3K9me3 marks were redeposited, and nuclear envelope tension was restored chromatin mobility returned to similar levels as in unperturbed cells. Another unique aspect of this study was the unorthodox timescale used in the particle tracking experiments and how SINK proved versatile enough to handle the challenge. This study validated both the consistency of SINK data with data from other more traditional methods and its adaptability to different experimental circumstances.

The common thread throughout this Thesis has been a demonstration of the broad range of applications, specificity, and timescale that the SINK method is capable of interrogating. Applications range from studying endogenous DNA damage from either ROS or mechanical stress, to differential response of various cell types to chemotherapy treatment, to understudied viral processes. Specificity can range from a single unique sequence of DNA, to particular

structures found throughout the nucleus, to hetero- or euchromatin generally, or even to the whole genome under all-out assault by a virus. Timescale is limited by what is practical for biological processes, but within that band SINK is easily customizable to fit the timescale of the process of interest. This work draws attention to the versatility of the SINK method and the richness that it can bring to the field of Mechanobiology.

## Future Outlook

This work demonstrates the wide range of utility of the SINK method for studying mechanical changes within cells and other processes that impact the mechanical properties of chromatin. We aimed to inspire creativity in the design of new experiments using SINK and confidence in this relatively new method.

In our examination of site-specific DNA damage, we noted a change in relative mobility between heterochromatic foci and the bulk average after damage was induced at the heterochromatic foci that was not observed in euchromatic foci. We stopped short, however, of identifying specific players in this change. Future work in determining the particular sensing mechanisms and chromatin remodeling pathways involved will be necessary to fully elucidate why and how this process occurs. We hypothesized that the increase in motion of damage foci located within heterochromatin to match the bulk average would allow greater access of repair machinery. This research focused primarily upon double strand breaks, but future SINK experiments could use repair factors unique to pathways that repair other types of DNA lesions as the chromatin bound probe for the purpose of determining whether this trend holds for all types of DNA insult or is unique to double strand breaks.

As demand for patient specific treatment of cancer increases, the importance of determining the exact mechanisms of both vulnerability and resistance of specific cell lines (as a model) or subpopulations of cells harvested from a biopsy (in clinical practice) to particular chemotherapy drugs will increase as well. Here, we validated SINK as a method to narrow the search. However, determining the mechanism connecting the observed loss of control over chromatin condensation to increased susceptibility to cisplatin was beyond the scope of this research. In future studies should start by cross-referencing factors involved in chromatin condensation with repair factors in the NER of NHEJ pathways to further narrow the search. Ultimately, sequencing would determine which factor(s) is/are defunct in MDA-MB-231 cells which potentially could lead to the discovery of new adjuvants to be used with cisplatin that would inhibit active versions of the factor(s) involved.

Our study of margination in HSV-1 infected cells hinted that the virus was activating one chromatin packaging pathway or another since the decrease in mobility preceded the formation of viral replication compartments. However, with the time and efficiency loss due to the COVID-19 pandemic, determining this pathway or the viral factor(s) involved in activating it fell outside the realm of practicality. Future work determining the players in this process could lead to the discovery of inhibitors that could prevent margination thereby halting lytic infections in their tracks.

The work presented in this Thesis has done much to demonstrate the versatility and effectiveness of the SINK method. However, the full potential of SINK has not yet fully been unlocked. Other students in the Dahl lab are working to improve SINK in various ways. Establishment of stably transduced cell lines expressing fluorescently tagged chromatin bound probes will ensure that future SINK experiments are more high-throughput and have much

higher n. Brighter fluorescent tags will mean imaging with lower intensity excitation which will lead to lower phototoxicity, and this will ease practical restrictions on the length and frequency of imaging. Fluorescent tags with narrower excitation bands means less chance of a bleeding effect from other channels and could potentially mean more channels may be imaged simultaneously. Improved streamlining of the SINK analysis workflow increases the speed of turnaround from experiment to final data and allows for larger data sets to be analyzed more quickly. All of these changes are well on their way and will continue to improve the robust utility of SINK. Furthermore, the power of SINK improves with the precision of the microscope, therefore those with access to confocal or super-resolution rigs will be able to push this method even further.